Effective shadowing of transition maps for a Hamiltonian saddle-center-center equilibrium. Part I: analytical results*

Amadeu Delshams†, Marian Gidea‡, and Pablo Roldan§

Abstract. We introduce a general methodology for constructing globally unstable trajectories near the normally hyperbolic invariant manifold (NHIM) of a saddle-center-center Hamiltonian equilibrium. We assume that the stable and unstable manifolds of the NHIM intersect transversally along homoclinic channels. The proposed approach builds upon the classical geometric mechanism of searching for trajectories near heteroclinic connections between invariant tori of the NHIM. The main ingredient is the Birkhoff normal form near the NHIM, which allows us to control the dynamics of the hyperbolic and center components. We construct transition maps on the NHIM that encode the dynamics along heteroclinic connections. By combining the transition maps with the inner dynamics, given by the restriction of the Hamiltonian flow to the NHIM, we show that these connections can be efficiently (in terms of travel time) shadowed by true trajectories of the full Hamiltonian system.

Key words. pseudotrajectories, shadowing, NHIM, Hamiltonian systems, homoclinic, heteroclinic orbits, invariant tori, normal forms, small divisors, transition map, scattering map, Arnol'd diffusion

MSC codes. 37C50 (Primary) 37C29, 37J40 (Secondary)

1. Introduction.

In 1964, Arnold [4] introduced the method of "transition chains" formed by transverse heteroclinic trajectories between invariant tori to prove the existence of global instability in Hamiltonian systems, a phenomenon that later received the name *Arnold diffusion*. Arnold's seminal work was extended through the introduction of geometric methods [16], based on the existence of a normally hyperbolic invariant manifold (NHIM), which acts as an organizing structure for the dynamics. Assuming that the stable and unstable manifolds of the NHIM intersect transversely along a homoclinic manifold, the dynamics can then be decomposed into an inner dynamics—corresponding to the restriction of the dynamics to the NHIM—and outer dynamics—corresponding to the dynamics along homoclinic orbits to the NHIM. The outer dynamics can be encoded in several ways. One way to encode the outer dynamics is via the *scattering map* [16], which relates the asymptotic past of a homoclinic point to its asymptotic future. Another way is via the *transition map* [21], which relates the projection onto the NHIM of the starting point of a homoclinic orbit segment to the projection onto the NHIM of the ending point of the segment. While the scattering map and the transition map are conjugated by the dynamics, the transition map offers the advantage of direct numerical computability. Computing the scattering map, by contrast, requires knowing both the transition map and the inner dynamics. In this paper, we focus on the transition map as our primary tool.

Combining the inner and the scattering maps, or the transition maps, one can construct diffusion pseudo-orbits. Finally, applying some shadowing lemmas, true diffusion trajectories of the system can be found. Geometric methods have been used to prove the existence of Arnold diffusion in different perturbative settings, where the scattering map can be computed explicitly to leading order. This is the case, for example, for "a priori unstable" Hamiltonian systems, which are systems close to integrable that already possess a NHIM [17, 18, 26, 27, 20, 29, 30, 35, 37, 11, 24, 31]. This is also the case for "a priori-chaotic" systems, which are perturbations of globally stable systems that possess a NHIM with transverse intersection of their invariant manifolds [16, 18, 34, 1, 15, 12]. There are also examples in celestial mechanics [28, 9, 13, 2, 14,

*Submitted to the editors Oct 26, 2026.

Funding: Research of M.G. was partially supported by NSF grant DMS-2154725 and DMS-2307718. Research of A.D and P.R. was partially supported by Spain's State Research Agency grant PID2024-158570NB-I00.

†Laboratory of Geometry and Dynamical Systems and IMTech, UPC.

‡Department of Mathematical Sciences, Yeshiva University.

§Departament de Matemàtiques, UPC. Corresponding author: Pablo.Roldan@upc.edu

7, 39].

In this paper, we consider a **non-perturbative** setting that is often encountered in applications, where the system parameters are fixed and specified in advance. If the same geometric structures are present (NHIM, transverse intersection of the stable and unstable manifolds), we may still consider the inner and scattering maps or transition maps, and use them to construct long pseudo-orbits that explore large regions of interest in the phase space. However, in the general case it is not possible to calculate these maps perturbatively; instead, one can perform a semi-analytical approximation [23].

Concretely, we consider a 3-degree-of-freedom Hamiltonian H with a saddle-center-center equilibrium point L, for which the corresponding center manifold has stable and unstable manifolds that intersect transversally. We parameterize the center manifold by a system of action-angle variables. In this context, we study global instability, specifically, we explicitly construct orbits along which one of the action variables varies significantly. As described in [3], a particularly relevant motivation and application is the SR3BP.

We now outline some of the main steps of the construction. Around the equilibrium point L, we introduce coordinates provided by the *Birkhoff normal form* (BNF for short, see Section 4 for full details) up to a given order M. This construction relies on a general non-resonance condition on the characteristic exponents of L up to order M. In these BNF coordinates, denoted by

$$(x, y, I, \phi) = (x, y, I_{\mathrm{p}}, I_{\mathrm{v}}, \phi_{\mathrm{p}}, \phi_{\mathrm{v}}) \in U = [-\delta, \delta]^2 \times [0, r]^2 \times \mathbb{T}^2, \tag{1.1}$$

the Hamiltonian H splits as $H = \mathcal{Z} + \mathcal{R} = \mathcal{Z}^{(M)} + \mathcal{R}^{(M)}$. The integrable part,

$$\mathcal{Z} = \mathcal{Z}(\boldsymbol{I}) = \mathcal{Z}(I_{\mathrm{s}}, I_{\mathrm{p}}, I_{\mathrm{v}}),$$

depends only on the actions $\boldsymbol{I} = (I_{\mathrm{s}}, I_{\mathrm{p}}, I_{\mathrm{v}})$, where $I_{\mathrm{s}} = xy$ represents the saddle component, with x and y being the conjugate saddle variables, and $I = (I_{\mathrm{p}}, I_{\mathrm{v}})$ are the two action variables, with conjugate angles $\phi = (\phi_{\mathrm{p}}, \phi_{\mathrm{v}})$. The subscripts s, p and v stand for the *saddle*, *planar*, and *vertical* components, respectively (the terminology is borrowed from the SR3BP framework). Consequently, the flow of the *truncated normal form* $\mathcal{Z}(\boldsymbol{I})$ can be integrated explicitly (see Section 4).

The term $\mathcal{R} = \mathcal{R}(M, \delta, r)$ is the *remainder*. We estimate its size within the domain U both analytically and numerically (see Sections 8, [3, Sections 5 and 6]), showing that it is typically negligible for practical and numerical purposes.

In BNF coordinates, the 4-dimensional (local) center manifold Λ is normally hyperbolic and is given by $x = y = 0$. A point $\boldsymbol{X} = (0, 0, I, \phi) \in \Lambda$ is parameterized by the two action variables $I = (I_{\mathrm{p}}, I_{\mathrm{v}})$ and the two conjugate angles $\phi = (\phi_{\mathrm{p}}, \phi_{\mathrm{v}})$. Furthermore, its 5-dimensional stable and unstable invariant manifolds are given by equations $x = 0$ and $y = 0$, respectively.

In our setting, neglecting the remainder $\mathcal{R}$ implies that the dynamics within Λ consist purely of angle translations along invariant tori. This recurrent behavior can be leveraged to reduce the dimensionality of the system through two steps. First, fixing the energy at $H = h$ isolates one of the action variables. For instance, the planar action can be expressed as $I_{\mathrm{p}} = f_h(I_{\mathrm{s}}, I_{\mathrm{v}})$ using the energy equation, which in BNF variables reads $\mathcal{Z}(I_{\mathrm{s}}, I_{\mathrm{p}}, I_{\mathrm{v}}) = h$. Let $U_h = U \cap \{H = h\}$ denote the BNF domain within the energy manifold, and $\Lambda_h = \Lambda \cap \{H = h\}$ the NHIM within this same energy manifold. Second, we eliminate one dimension by choosing an appropriate section within U_h, namely $\Sigma = \{\phi_{\mathrm{p}} = 0\}$.

This allows us to restrict the dynamics to a 4-dimensional *reduced phase space* defined as $U_h^\Sigma := U_h \cap \Sigma$:

$$U_h^\Sigma = \{\boldsymbol{k} = (x, y, I, \phi) : I_{\mathrm{p}} = f_h(I_{\mathrm{s}}, I_{\mathrm{v}}), \phi_{\mathrm{p}} = 0, (x, y) \in [-\delta, \delta]^2, I_{\mathrm{v}} \in [0, r], \phi_{\mathrm{v}} \in \mathbb{T}\}, \tag{1.2}$$

which is parameterized by $(x, y, I_{\mathrm{v}}, \phi_{\mathrm{v}})$. The dynamics on U_h^Σ is described by the first return map $\mathcal{F}$ of the Hamiltonian flow, which is a symplectic diffeomorphism with respect to the symplectic form $dy \wedge dx + dI_{\mathrm{v}} \wedge d\phi_{\mathrm{v}}$.

Embedded within U_h^Σ is the two-dimensional *reduced NHIM*

$$\Lambda_h^\Sigma := \Lambda_h \cap \Sigma = \{\boldsymbol{x} = (0, 0, I, \phi) : I_{\mathrm{p}} = f_h(0, I_{\mathrm{v}}), \phi_{\mathrm{p}} = 0, I_{\mathrm{v}} \in [0, r], \phi_{\mathrm{v}} \in \mathbb{T}\}\,, \tag{1.3}$$

which is parameterized solely by $(I_{\mathrm{v}}, \phi_{\mathrm{v}})$. We denote by f the restriction of the first return map $\mathcal{F}$ to Λ_h^Σ.

Then, a semi-analytical computation of the *transition map* [21] can be performed. In this paper, we employ the transition map $\mathcal{T}$ and the reduced transition map τ instead of the scattering map $\mathcal{S}$ and the reduced scattering map σ used in [21, 23]. Although both maps are conjugate by the flow (see Section 2) and play a similar role, they differ fundamentally in their temporal scales: the transition map encodes finite-time homoclinic segments, whereas the scattering map encodes infinite-time homoclinic orbits (see Definition 2.2). Consequently, the transition map implicitly preserves information on the transition time of each homoclinic segment, which is absent in the scattering map. This temporal information is crucial for tracking the total duration of pseudo-orbits. Note that obtaining sharp estimates on diffusion times is notoriously difficult (see, for instance, [6, 5, 43, 30] and references therein).

Moreover, the transition map can be directly obtained from the numerical procedure to compute homoclinic trajectories, while the scattering map is indirectly obtained from the transition map (see Section 5). We expect that numerical analysts will prefer the transition map, as it remains closer to computations.

In our context, we obtain several transition maps $\{\tau_1, \dots, \tau_L\}$ associated to different families of homoclinic segments. Then, we consider the Iterated Function System (IFS) $\{f, \tau_1, \dots, \tau_L\}$, formed by the transition maps and the inner map. We construct orbits of the IFS along which the vertical action I_{v} undergoes some significant gain. Then we develop some *efficient shadowing* strategies (see Section 3) that provide true trajectories that achieve the same gain (up to a small error). In particular, we consider a simple situation (motivated by applications) in which the IFS consists only of transition maps and not inner maps. Theorem 3.1 and Theorem 3.2 guarantee the existence of true orbits that shadow a given orbit of the IFS $\{\tau_1, \dots, \tau_L\}$.

The shadowing strategies presented in Section 3 significantly improve existing shadowing theorems in the literature (such as, among others, [33, 17, 34, 36]). While those classical results establish the existence of shadowing orbits, they generally lack a constructive procedure to locate them. Furthermore, they typically require a large number of iterations, which translates into excessively long integration times in the original Hamiltonian system.

In contrast, by leveraging the BNF to approximate the motion near the NHIM, our shadowing lemmas in Section 3 are *constructive* and *efficient*. Here, *efficiency* implies that the travel time along the true trajectories closely matches that of the IFS orbits. This approach shares similarities with the shadowing method in [34], which utilizes Fenichel normal form.

To distinguish the IFS orbits from the true trajectories of the system, we will refer to the former as *guiding orbits*. In our setting, a guiding orbit of an iterated function system (IFS) with dynamics $\{f, \tau_1, \dots, \tau_L\}$ is simply a finite sequence $(\boldsymbol{x}_i)_{i=1}^N$ of points in the two-dimensional reduced NHIM Λ_h^Σ, where each iterate satisfies one of the following conditions:

- **Inner map:** $\boldsymbol{x}_{i+1} = f(\boldsymbol{x}_i)$. This map models a "complete revolution" of the vertical angle ϕ_{v} from 0 to 2π within Λ_h^Σ, during which the vertical action I_{v} remains constant.
- **Transition map:** $\boldsymbol{x}_{i+1} = \tau_j(\boldsymbol{x}_i)$ for some $j = 1, \dots, L$. This map governs the evolution along a segment of a homoclinic orbit to Λ_h^Σ, along which I_{v} may vary.

The companion paper [3] illustrates the efficiency of this methodology in the case of the NHIM associated to the libration point L_1 of the Spatial Restricted 3-Body Problem (SR3BP) for the Sun-Earth system.

2. Preliminaries.

2.1. Scattering map. We recall the definition of the scattering map following [19]. We consider a general setting of flow Φ_t on a manifold M, and assume that there is a normally

hyperbolic invariant manifold Λ for the flow. Associated to Λ we have stable and unstable manifolds, $W^s(\Lambda)$ and $W^u(\Lambda)$, which are foliated by stable and unstable leaves $W^s(\Lambda) = \bigcup_{\boldsymbol{y}\in\Lambda} W^s_{\boldsymbol{y}}$ and $W^u(\Lambda) = \bigcup_{\boldsymbol{y}\in\Lambda} W^u_{\boldsymbol{y}}$. The canonical projections along the leaves are defined as follows: $\Omega_+ : W^s(\Lambda) \to \Lambda$ is given by $\Omega_+(\boldsymbol{x}) = \boldsymbol{x}^{\mathrm{s}}$ provided that $\boldsymbol{x} \in W^s(\boldsymbol{x}^{\mathrm{s}})$ and $\Omega_- : W^u(\Lambda) \to \Lambda$ is given by $\Omega_-(\boldsymbol{x}) = \boldsymbol{x}^{\mathrm{u}}$ provided that $\boldsymbol{x} \in W^u(\boldsymbol{x}^{\mathrm{u}})$.

We will implicitly assume that the the manifold M, the flow Φ_t, as well as the NHIM Λ and the related geometric structures described above are differentiable enough.

Suppose that $W^s(\Lambda)$ and $W^u(\Lambda)$ intersect transversally along a homoclinic manifold Γ, that is, for each $\boldsymbol{x} \in \Gamma \subseteq W^u(\Lambda) \cap W^s(\Lambda)$, we have

$$\begin{aligned} T_{\boldsymbol{x}}M &= T_{\boldsymbol{x}}W^u(\Lambda) + T_{\boldsymbol{x}}W^s(\Lambda), \\ T_{\boldsymbol{x}}\Gamma &= T_{\boldsymbol{x}}W^u(\Lambda) \cap T_{\boldsymbol{x}}W^s(\Lambda). \end{aligned}$$

and moreover, the following strong transversality condition holds:

$$\begin{aligned} T_{\boldsymbol{x}}W^s(\Lambda) &= T_{\boldsymbol{x}}W^s(\boldsymbol{x}_+) \oplus T_{\boldsymbol{x}}(\Gamma), \\ T_{\boldsymbol{x}}W^u(\Lambda) &= T_{\boldsymbol{x}}W^u(\boldsymbol{x}_-) \oplus T_{\boldsymbol{x}}(\Gamma). \end{aligned}$$

Then, the restrictions Ω^Γ_+, Ω^Γ_- of Ω_+, Ω_-, respectively, to Γ are local diffeomorphisms. If Γ is so that Ω^Γ_+, Ω^Γ_- are diffeomorphisms onto their images, then it is referred to as a *homoclinic channel*.

When we flow the homoclinic channel Γ to $\Phi_t(\Gamma)$, $t \in \mathbb{R}$, the corresponding wave maps are conjugate by the flow, i.e.,

$$\Omega^{\Phi_t(\Gamma)}_+ = \Phi_t \circ \Omega^\Gamma_+ \circ \Phi_{-t}. \tag{2.1}$$

Definition 2.1. *Given a homoclinic channel Γ, the scattering map associated to Γ is a diffeomorphism from $Dom(\mathcal{S}^\Gamma) := \Omega^\Gamma_-(\Gamma) \subseteq \Lambda$ to $Im(\mathcal{S}^\Gamma) := \Omega^\Gamma_+(\Gamma) \subseteq \Lambda$ given by*

$$\mathcal{S}^\Gamma = \Omega^\Gamma_+ \circ (\Omega^\Gamma_-)^{-1}.$$

The scattering map depends on the choice of the homoclinic channel Γ. In general, its domain and range are proper subsets of Λ.

From Definition 2.1 it follows that, if $\boldsymbol{x} \in \Gamma$ is a homoclinic point and

$$\mathcal{S}^\Gamma(\boldsymbol{x}^{\mathrm{u}}) = \boldsymbol{x}^{\mathrm{s}}, \text{ where } \boldsymbol{x}^{\mathrm{u,s}} \in \Lambda,$$

then

$$\begin{aligned} d(\Phi_{-t_-}(\boldsymbol{x}), \Phi_{-t_-}(\boldsymbol{x}^{\mathrm{u}})) &\to 0, \text{ as } t_- \to \infty, \\ d(\Phi_{t_+}(\boldsymbol{x}), \Phi_{t_+}(\boldsymbol{x}^{\mathrm{s}})) &\to 0, \text{ as } t_+ \to \infty. \end{aligned}$$

A remarkable property of the scattering map is that it is (exact) symplectic, provided that the manifold M and the flow Φ_t are (exact) symplectic. We refer to [19] for details.

When we flow the homoclinic channel Γ to $\Phi_t(\Gamma)$, it follows from (2.1) that the corresponding scattering maps are conjugate by the flow, so we have the following invariance property

$$\mathcal{S}^{\Phi_t(\Gamma)} = \Phi_t \circ \mathcal{S}^\Gamma \circ \Phi_{-t}, \tag{2.2}$$

for $t \in \mathbb{R}$. We note that on the right-hand side the above, the flow Φ_t acts on Λ.

2.2. Transition map. We now recall the *transition map* (see [19]).

Definition 2.2. *Given a homoclinic channel* Γ *and (sufficiently large) times* T_-, T_+*, the transition map* $\mathcal{T} = \mathcal{T}^{\Gamma}_{T_-,T_+} : \Phi_{-T_-}(Dom(\mathcal{S}^{\Gamma})) \to \Phi_{T_+}(Im(\mathcal{S}^{\Gamma}))$ *is given by*

$$\mathcal{T} = \Phi_{T_+} \circ \mathcal{S}^{\Gamma} \circ \Phi_{T_-}. \tag{2.3}$$

We write $\mathcal{T}(\boldsymbol{x}_-) = \boldsymbol{x}_+$.

Remark 2.3. In Definition 2.2 the times T_+, T_- are fixed. More generally, we can consider T_+, T_- as continuous functions on Γ. In Section 5, given a neighborhood U of the NHIM Λ, and Σ_+, Σ_- two surfaces of section inside U, for any $\boldsymbol{x} \in \Gamma$ we will define $T_- = T_-(\boldsymbol{x})$ as the first time $t > 0$ when $\Phi_{-t}(\boldsymbol{x}) \in \Sigma_-$, and $T_+ = T_+(\boldsymbol{x})$ as the first time $t > 0$ when $\Phi_t(\boldsymbol{x}) \in \Sigma_+$.

Since both the scattering map and the inner dynamics are (exact) symplectic, it follows that the transition map is also (exact) symplectic.

Using the conjugacy (2.1), the transition map can also be written

$$\mathcal{T} = \Omega^{\Gamma_+}_+ \circ \Phi_{T_+} \circ \Phi_{T_-} \circ \left(\Omega^{\Gamma_-}_-\right)^{-1}, \tag{2.4}$$

where we have introduced $\Gamma_+ := \Phi_{T_+}(\Gamma)$ and $\Gamma_- := \Phi_{-T_-}(\Gamma)$. This will be used in Section 5 to compute the transition map, because the local wave maps $\Omega^{\Gamma_\pm}_\pm$ have particularly simple expressions in BNF coordinates.

Now we consider the case of a discrete-time dynamical system, given by a diffeomorphism $\mathcal{F}$ on M. Let Λ be a NHIM for $\mathcal{F}$, and let f denote the restriction of $\mathcal{F}$ to Λ. Let Γ be a homoclinic channel.

Then the scattering map σ^{Γ} can be defined in a similar way to the flow case.

The invariance property (2.2) becomes:

$$\sigma^{f(\Gamma)} = f \circ \sigma^{\Gamma} \circ f^{-1}.$$

The transition map $\tau = \tau^{\Gamma}_{m,n}$ can be defined in a similar way to the flow case, i.e.,

$$\tau = f^m \circ \sigma^{\Gamma} \circ f^n,$$

for $m, n > 0$ sufficiently large.

Using the invariance of the scattering map we obtain

$$\tau^{\Gamma}_{m,n} = f^m \circ \sigma^{\Gamma} \circ f^n = f^{m-1} \circ \sigma^{\mathcal{F}(\Gamma)} \circ f^{n+1} = \tau^{\mathcal{F}(\Gamma)}_{m-1,n+1}.$$

It follows:

$$\tau^{\Gamma}_{m,n} = \tau^{\mathcal{F}^k(\Gamma)}_{m-k,n+k},$$

for any $k \in \mathbb{Z}$.

2.3. Shadowing lemmas. Let Λ be a NHIM for $\mathcal{F}$, $f = \mathcal{F}_{|\Lambda}$ and σ_α, $\alpha \in \{1, \dots, L\}$, be a finite collection of scattering maps. (We omit the homoclinic channel from the notation.)

We assume that there is a neighborhood $\mathcal{U}$ of Λ on which there is as system of coordinates (x, y, θ) with the following properties:

$$\begin{aligned}
\Lambda &= \{(x, y, \theta) \,:\, x = y = 0\},\\
W^u(\Lambda) &= \{(x, y, \theta) \,:\, y = 0\},\\
W^s(\Lambda) &= \{(x, y, \theta) \,:\, x = 0\},\\
W^u(\boldsymbol{x}) &= \{(x, y, \theta) \,:\, y = 0,\, \theta = \theta(\boldsymbol{x})\} \text{ for } \boldsymbol{x} \in \Lambda,\\
W^s(\boldsymbol{x}) &= \{(x, y, \theta) \,:\, x = 0,\, \theta = \theta(\boldsymbol{x})\} \text{ for } \boldsymbol{x} \in \Lambda.
\end{aligned} \tag{2.5}$$

Remark 2.4. In the context of Sections 4 and 5, the coordinates (x, y, θ) represent the normal form coordinates (x, y, I, ϕ)—with $\theta = (I, \phi)$—as described in (1.2).

We consider a sequence of transition maps τ_i, $i = 1, ..., N-1$, where

$$\tau_i = f^{m_i} \circ \sigma_{\alpha(i)} \circ f^{n_i},$$

for some scattering map $\sigma_{\alpha(i)}$ with $\alpha(i) \in \{1, \dots, L\}$ and some $m_i, n_i > 0$. Each transition map τ_i depends on both the scattering map σ_{α_i} and the orders of iterates m_i, n_i. Hence, one can have $\tau_i = \tau_j$ for some $i \neq j$. We denote by $M_i := m_i + n_i$ the number of iterates associated to the transition map τ_i.

Let

$$\boldsymbol{x}_1, \boldsymbol{x}_2 \dots, \boldsymbol{x}_N$$

be a guiding orbit in Λ of the transition maps $\tau_1, \dots, \tau_{N-1}$, in the sense that

$$\tau_i(\boldsymbol{x}_i) = \boldsymbol{x}_{i+1} \text{ for } i = 1, \dots, N-1.$$

Remark 2.5. Above, we implicitly assume that the range of τ_i intersects the domain of τ_{i+1}, for $i = 0, \dots, N-1$. In the context of the SR3BP, this is automatically satisfied since the scattering map and the corresponding transition maps are globally defined. See [3, Section 7.1]

Lemma 2.6. *Let σ_α be a family of scattering maps with associated homoclinic channels Γ_α, for $\alpha \in \{1, \dots, L\}$.*

For every $\varepsilon > 0$ there exists $M_{\min} < M_{\max}$ such that, if

$$\tau_i = f^{m_i} \circ \sigma_{\alpha(i)} \circ f^{n_i}, i = 1, \dots, N-1,$$

is a transition map associated with the homoclinic channel $\Gamma_{\alpha(i)}$, and with m_i, n_i satisfying $M_{\min} \leq M_i = m_i + n_i \leq M_{\max}$, and if

$$\boldsymbol{x}_{i+1} = \tau_i(\boldsymbol{x}_i), \text{ for } i = 1, \dots, N-1,$$

then there exists a point $\boldsymbol{y}_1$ whose orbit $\boldsymbol{y}_1, \dots, \boldsymbol{y}_N$ ε-shadows $\boldsymbol{x}_1, \boldsymbol{x}_2, \dots, \boldsymbol{x}_N$ in the sense

$$\begin{aligned} \boldsymbol{y}_{i+1} =& \mathcal{F}^{M_i}(\boldsymbol{y}_i), \text{ and} \\ d(\boldsymbol{y}_i, \boldsymbol{x}_i) <& \varepsilon \text{ for } i = 1, \dots, N. \end{aligned}$$

The orbit $\boldsymbol{y}_1, \dots, \boldsymbol{y}_N$ is a true orbit of the system. The number of iterates to take $\boldsymbol{y}_i$ to $\boldsymbol{y}_{i+1}$ is $M_i = m_i + n_i$, which is the same as the number of iterates associated to the transition map τ_i.

In particular, we can choose the number of iterates $m_i = m_*$, $n_i = n_*$, and $M_i = M_*$ to be independent of i.

The proof of this lemma will be given in Section 7.

Remark 2.7. We compare Lemma 2.6 with some similar shadowing lemma type of results. The paper [36] provides a result on shadowing orbits generated by scattering maps on a NHIM. The argument requires that the dynamics restricted to the NHIM satisfies Poincaré recurrence and, therefore, the shadowing orbits may take a long time. Another result in the paper is on shadowing orbits obtained by alternately applying scattering maps and iterates of the inner dynamics. While this result does not require Poincaré recurrence, it requires that the number of iterates at each step is sufficiently large with respect to the number of iterates at all previous steps. A similar result to the latter appears in [34]. Our Lemma 2.6 concerns shadowing orbits of transition maps and gives a uniform number of iterates of the inner dynamics. Since the transition map also encodes the effect of the inner dynamics, and we require that the input of each transition map coincides with the output of the preceding transition map, there is no need to invoke recurrence. However, this lemma only allows for the shadowing of finite orbits.

3. Main results. Some of the standard shadowing results about finding true trajectories that follow given pseudo-orbits are not practical for concrete applications. On the one hand, the existence of the true trajectories is not constructive and, on the other hand, the theoretical shadowing results may involve a large number of iterations, which translates into an enormous time in the original Hamiltonian.

The main objective of this paper is to provide a *constructive* and *efficient* shadowing of the guiding orbits.

The first shadowing result is achieved by using Birkhoff Normal Form (BNF) variables within the domain U (4.2), where the reduced NHIM Λ_h^Σ takes the form (1.3) and the associated reduced transition maps are defined. Outside U, the candidates for drift trajectories are N orbit segments that exit U through the unstable (outgoing) section $\Sigma_- = \{x = \pm\delta\}$ and return to U through the stable (incoming) section $\Sigma_+ = \{y = \pm\delta\}$, traveling close to the selected homoclinic trajectories to the NHIM Λ. Note that the drift trajectories constructed in Theorem 3.1 (below) are not arbitrarily close to the guiding orbit—as is the case in standard shadowing lemmas—but are instead only δ-close. This restriction minimizes the drift time, matching the duration spent along the homoclinic segments that generate the guiding orbit.

Moreover, to obtain drift trajectories with the shortest travel time, we consider in Theorem 3.1 guiding orbits formed exclusively by iterations of transition maps. Consequently, we seek trajectories that cross the section Σ only once inside U, which implies they will not remain too close to the NHIM. Thus, to guarantee a proper return, we impose the *homecoming condition* (6.4):

$$(N-1)\chi < 2\pi\lambda/\nu_{\mathrm{p}},$$

where the saddle exponent $\lambda = \dfrac{\partial \mathcal{Z}}{\partial I_{\mathrm{s}}}$ and the planar frequency $\nu_{\mathrm{p}} = \dfrac{\partial \mathcal{Z}}{\partial I_{\mathrm{p}}}$ are introduced in equations (4.3–4.5), whereas e^χ is a uniform bound for the maximum of the derivatives of the exterior Poincaré maps $P_{\mathrm{ext}}^j : \Sigma_- \to \Sigma_+$ associated with the transition maps τ_j for $1 \le j \le L$.

Theorem 3.1 (Analytical shadowing of a guiding orbit of transition maps). *Let $(\boldsymbol{x}_i)_{i=1}^N$ be a guiding orbit of the iterated function system (IFS) defined on the reduced NHIM Λ_h^Σ (1.3) generated **solely** by $L \ge 1$ reduced transition maps $\{\tau_1, \dots, \tau_L\}$, expressed in BNF coordinates (1.1). Let δ be the size of the saddle variables (1.2) within the BNF domain U, and assume that the* homecoming condition (6.4) *holds.*

Then, there exists a true trajectory $\Phi_t(\mathbf{x})$ of the system that δ-shadows the guiding orbit. Specifically, there exists a strictly increasing sequence of times $0 < t_1 < \cdots < t_N$ such that

$$\|\Phi_{t_i}(\mathbf{x}) - \boldsymbol{x}_i\| \le \delta \quad \text{for all } i = 1, \dots, N.$$

Moreover, if the guiding orbit $(\boldsymbol{x}_i)_{i=1}^N$ is generated by a sequence of homoclinic segments $\left[\boldsymbol{z}_i^-, \boldsymbol{z}_{i+1}^+\right]$, where $\boldsymbol{z}_i^- \in W^{\mathrm{u}}(\boldsymbol{x}_i) \cap \Lambda_h^\Sigma$ and $\boldsymbol{z}_{i+1}^+ = \Phi_{\boldsymbol{T}^i}\left(\boldsymbol{z}_i^-\right) \in W^{\mathrm{s}}(\boldsymbol{x}_{i+1}) \cap \Lambda_h^\Sigma$, then each t_i can be chosen as $t_i = \boldsymbol{T}^1 + \cdots + \boldsymbol{T}^i$, yielding a total drift time of $t_N = \boldsymbol{T}^1 + \cdots + \boldsymbol{T}^N$.

In Section 6, we present a direct analytical proof for the construction of this shadowing trajectory. Our approach relies fundamentally on the transition map and the BNF; these tools enables us to obtain an optimal time estimate that matches the duration given by the sequence of homoclinic segments associated to the guiding orbit.

General guiding orbits are composed of transition maps and inner maps. Because each inner map adds a revolution around the NHIM, these guiding orbits do not generally provide optimal drift time estimates.

Theorem 3.1 provides an efficient shadowing of a given guiding orbit. In particular, the shadowing orbits spend little time near the NHIM (they cross the section Σ only once inside U). However, the error in the shadowing equals the size δ of the BNF neighborhood, which can be large.

Theorem 3.2 below provides an alternative shadowing result that minimizes the shadowing error. If we ignore the "effects of the truncation error" $\epsilon_M = \epsilon_M(\delta)$ given by (8.3), for any "mathematical error" ε it gives a threshold value on the number of iterates of the inner map that are required by the transition maps. Then, any orbit generated by such transition maps can be shadowed within a ε-mathematical error (to which we have to add the effects of the truncation.) However, if ε is small, the shadowing orbits may spend a long time near the NHIM (they may cross the section Σ multiple times inside U).

Theorem 3.2 (Topological shadowing of a guiding orbit of transition maps).
Let $\epsilon_M = \epsilon_M(\delta)$ denote the effect of truncation error (8.3) of the transformation to BNF variables.

Then, for every $\epsilon > 0$ there exist m_*, n_* sufficiently large and a constant $C > 0$, such that, for any guiding orbit $(\boldsymbol{x}_i)_{i=1}^N$ given by

$$\boldsymbol{x}_{i+1} = \tau_i(\boldsymbol{x}_i), \ \text{for } i = 1, \dots, N-1,$$

where each transition map τ_i is of the form

$$\tau_i = f^{m_*} \circ \sigma_{\alpha(i)} \circ f^{n_*},$$

there exists a true trajectory $\Phi_t(\boldsymbol{x})$ that $(\varepsilon + C\epsilon_M)$-shadows the guiding orbit,

$$\|\Phi_{t_i}(\boldsymbol{x}) - \boldsymbol{x}_i\| \le \epsilon + C\epsilon_M \quad \text{for all } i = 1, \dots, N,$$

for some strictly increasing sequence of times $0 < t_1 < \cdots < t_N$.

The proof is given in Section 7.

4. Birkhoff normal form (BNF). Around a saddle-center-center equilibrium point of a Hamiltonian system, the parameterization method provides an efficient framework to compute the local center, center-stable and center-unstable manifolds, see, e.g., [8, 41]. Alternatively, the classical Birkhoff normal form (BNF), (see, e.g., [38, 25, 40]), or its variants, such as resonant or saddle normal forms [42], can be employed. Notably, these normal form approaches offer the additional advantage of approximating the full flow in a neighborhood of the equilibrium point.

Let V be a neighborhood of a saddle-center-center point L of a three degrees of freedom Hamiltonian $H(X, Y, Z, P_X, P_Y, P_Z)$ where the BNF up to some order M is computed, and let

$$\boldsymbol{K} = (x, y, I, \phi) \in U \mapsto (X, Y, Z, P_X, P_Y, P_Z) = \mathcal{K} = \Psi(\boldsymbol{K}) \in V = \Psi(U), \tag{4.1}$$

where $I = (I_\mathrm{p}, I_\mathrm{v})$ and $\phi = (\phi_\mathrm{p}, \phi_\mathrm{v})$, be a symplectic transformation with respect to the symplectic forms $dx \wedge dy + d\phi_\mathrm{p} \wedge dI_\mathrm{p} + d\phi_\mathrm{v} \wedge dI_\mathrm{v}$ on U and $dX \wedge dP_X + dY \wedge dP_Y + dZ \wedge dP_Z$ on V, where

$$U = U(\delta, r) = \left\{ \boldsymbol{K} = (x, y, I, \phi) \in [-\delta, \delta]^2 \times [0, r]^2 \times \mathbb{T}^2 \right\}. \tag{4.2}$$

The transformation $\Psi = \Psi^{(M)}$ is such that $H \circ \Psi = \mathcal{Z}(\boldsymbol{I}) + \mathcal{R} = \mathcal{Z}^{(M)}(\boldsymbol{I}) + \mathcal{R}^{(M)}$, where $\boldsymbol{I} := (I_\mathrm{s}, I)$, $I_\mathrm{s} := xy$, $I := (I_\mathrm{p}, I_\mathrm{v})$ are three first integrals in involution of the normal form $\mathcal{Z}(I_\mathrm{s}, I)$, $\phi := (\phi_\mathrm{p}, \phi_\mathrm{v})$ are the conjugate angles to the two actions I, and $\mathcal{R}$ is the remainder.

The normalized Hamiltonian expands as

$$\mathcal{Z}(\boldsymbol{I}) = h^0 + \lambda^0 I_\mathrm{s} + \nu^0 \cdot I + O_2(\boldsymbol{I}), \ \text{with } \nu^0 \cdot I = \nu^0_\mathrm{p} I_\mathrm{p} + \nu^0_\mathrm{v} I_\mathrm{v},$$

where λ^0 is the saddle characteristic exponent at the equilibrium L, while ν^0_p, ν^0_v are the planar and vertical frequencies at L. For definiteness, we will assume that $h^0, \lambda^0, \nu^0_\mathrm{p}, \nu^0_\mathrm{v} > 0$. Note that Ψ is a genuine coordinate change (i.e., a diffeomorphism) for $I_\mathrm{p} > 0$ and $I_\mathrm{v} > 0$. In particular, as is usual when considering polar coordinates, the BNF coordinates are degenerate

at the equilibrium point L, which is given by $x = y = I_{\rm p} = I_{\rm v} = 0$ for arbitrary angles $\phi_{\rm p}$ and $\phi_{\rm v}$. Note also that, for simplicity, we are considering the same domain for the saddle variables x, y, and respectively for the actions $I_{\rm p}$ and $I_{\rm v}$.

The main feature of the BNF is that often, by choosing the order M appropriately in terms of the parameters $\lambda^0, \nu_{\rm p}^0, \nu_{\rm v}^0$, and the sizes δ, r of the neighborhood U introduced in equation (4.2), the remainder $\mathcal{R}$ is so small that it can be neglected for practical purposes, and therefore we have a complete and explicit description of the local motion around the equilibrium point.

In fact, the BNF of order M can only be used in the absence of resonances between the characteristic exponents of the equilibrium point of order less than or equal to M, that is, when $\left|k_0\lambda^0 + \mathrm{i}\, k_{\rm p}\nu_{\rm p}^0 + \mathrm{i}\, k_{\rm v}\nu_{\rm v}^0\right|$ is not too small for integers k_0, $k_{\rm p}$, $k_{\rm v}$ such that $|k_0| + |k_{\rm p}| + |k_{\rm v}| \le M$, which is what will be assumed in this paper. In case of resonances of small order, a resonant normal form should be used. See more details in Section 4.

Let us now be more precise. If we neglect the remainder $\mathcal{R}$, the flow inside U is simply given by the normal form $\mathcal{Z}(\boldsymbol{I})$, with $\boldsymbol{I} = (I_{\rm s}, I)$, where $I_{\rm s} = xy$, $I = (I_{\rm p}, I_{\rm v})$ are conserved quantities. Abusing notation, we will also denote the BNF flow by Φ_t. It takes the explicit form

$$x(t) = \mathrm{e}^{t\lambda}x(0), \quad y(t) = \mathrm{e}^{-t\lambda}y(0), \qquad I(t) = I(0), \quad \phi(t) = \phi(0) + t\nu, \tag{4.3}$$

with $\phi = (\phi_{\rm p}, \phi_{\rm v})$, where we have introduced the notation

$$\lambda := \frac{\partial \mathcal{Z}}{\partial I_{\rm s}} = \frac{\partial \mathcal{Z}}{\partial I_{\rm s}}(\boldsymbol{I}) = \lambda^0 + O(\boldsymbol{I}) = \frac{\partial \mathcal{Z}}{\partial I_{\rm s}}(\boldsymbol{I}(0)), \tag{4.4}$$

$$\nu := \frac{\partial \mathcal{Z}}{\partial I} = \nabla_I \mathcal{Z}(\boldsymbol{I}) = \nu^0 + O(\boldsymbol{I}) = \nabla_I \mathcal{Z}(\boldsymbol{I}(0)). \tag{4.5}$$

Notice that, restricting δ and r if necessary, $\lambda > 0$ for $-\delta^2 \le I_{\rm s} \le \delta^2$, $0 \le I_{\rm p}, I_{\rm v} \le r$.

Thanks to the explicit expression (4.3) for the trajectories in U, the description of the most important invariants sets within U, the NHIM, their invariants manifolds, as well as the rest of trajectories, is straigthforward.

First, let us denote

$$\Lambda = W^{\rm c}_{\rm loc} = \{\boldsymbol{X} = (x = 0, y = 0, I, \phi\} = \{(0, 0, I, \phi)\} = \{(0, 0)\} \times [0, r]^2 \times \mathbb{T}^2$$

the local center manifold of L provided by the normal form, which is a 4-dimensional NHIM. The dynamics inside Λ is simply determined by $\dot I = 0, \dot\phi = \nu$, where $\nu = \nu(0, I)$, and given by $\Phi_t(\boldsymbol{X}) = (0, 0, I, \phi + t\nu)$.

Any point $\boldsymbol{X} = (0, 0, I, \phi) \in \Lambda$ has associated *local stable and unstable fibers* in U

$$W^{\rm s}_{\rm loc}(\boldsymbol{X}) = \{\boldsymbol{Z} = (x = 0, y, I, \phi),\ |y| \le \delta\}, \ W^{\rm u}_{\rm loc}(\boldsymbol{X}) = \{\boldsymbol{Z} = (x, y = 0, I, \phi),\ |x| \le \delta\},$$

which can be extended outside U by the backward and forward flow, respectively, to form the global stable and unstable fibers $W^{\rm s}(\boldsymbol{X})$ and $W^{\rm u}(\boldsymbol{X})$. Their unions on $\boldsymbol{X} \in \Lambda$ form the stable and unstable *invariant* manifolds of the NHIM Λ

$$W^{\rm s}(\Lambda) = \bigcup_{\boldsymbol{X}\in\Lambda} W^{\rm s}(\boldsymbol{X}), \qquad W^{\rm u}(\Lambda) = \bigcup_{\boldsymbol{X}\in\Lambda} W^{\rm u}(\boldsymbol{X}).$$

The dynamics inside $W^{\rm s}_{\rm loc}(\Lambda)$ is simply determined by

$$\dot y = -\lambda y, \quad \dot\phi = \nu,$$

where $\lambda = \lambda(0, I)$ and $\nu = \nu(0, I)$, and given by $\Phi_t(\boldsymbol{Z}) = \left(0, \mathrm{e}^{-\lambda t}y, I, \phi + t\nu\right)$ for $Z = (0, y, I, \phi) \in W^{\rm s}_{\rm loc}(\Lambda)$. With the same $\lambda = \lambda(0, I)$ and $\nu = \nu(0, I)$, the dynamics inside $W^{\rm u}_{\rm loc}(\Lambda)$ is determined by

$$\dot x = \lambda x, \quad \dot\phi = \nu,$$

and given by $\Phi_t(\boldsymbol{Z}) = \left(\mathrm{e}^{\lambda t}x, 0, I, \phi + t\nu\right)$ for $Z = (x, 0, I, \phi) \in W^{\rm u}_{\rm loc}(\Lambda)$.

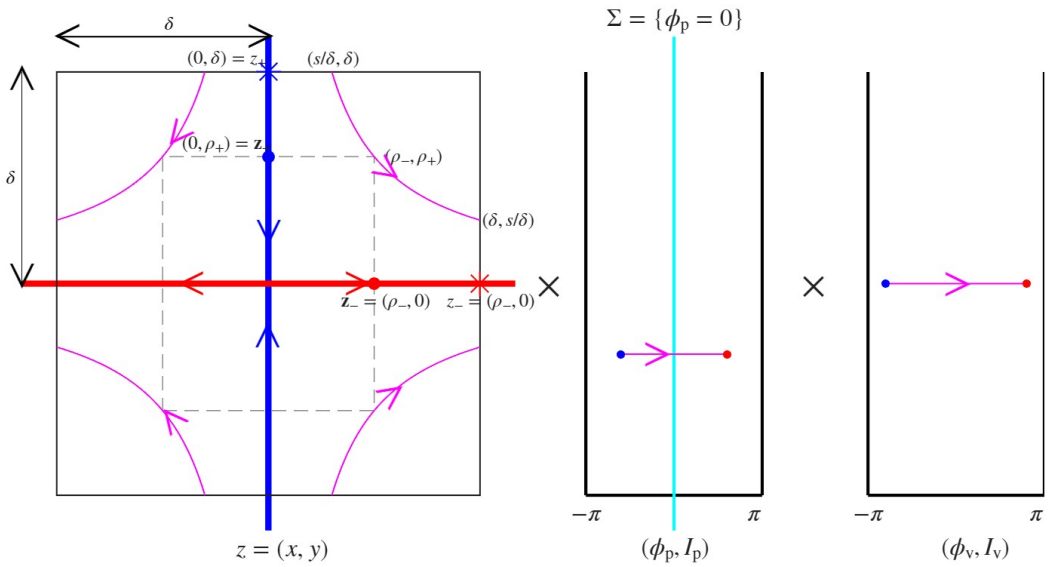


Figure 1: $\boldsymbol{Z}_+ = (z_+, I, \phi) = (0, \delta, I_+, \phi_+)$, $\boldsymbol{K}_+ = (s/\delta, \delta, I, \phi_+)$, $\boldsymbol{Z}_- = (z_-, I, \phi) = (\delta, 0, I_-, \phi_-)$, $\boldsymbol{K}_- = (\delta, s/\delta, I, \phi_-)$, $\boldsymbol{z}_+ = (\mathbf{z}_+, I, \phi) = (0, \rho_+, I, \phi)$, $\boldsymbol{z}_- = (\mathbf{z}_-, I, \phi) = (\rho_-, 0, I, \phi)$, $\boldsymbol{k} = (\rho_-, \rho_+, I, \phi)$. In this figure the trajectory from $\boldsymbol{K}_+$ to $\boldsymbol{K}_-$ only crosses once the section $\Sigma = \{\phi_{\mathrm{p}} = 0\}$, so that $\boldsymbol{k} = \boldsymbol{k}_+ = \boldsymbol{k}_-$. See the text for more information.

Definition 4.1 (Sections). *We define the following local Poincaré sections for the flow. The* incoming boundary *is given by* $\Sigma_+ := \{\boldsymbol{K} = (x, y, I, \phi) \in \partial U : y = \pm\delta\}$, *while the* outgoing boundary *is given by* $\Sigma_- := \{\boldsymbol{K} = (x, y, I, \phi) \in \partial U : x = \pm\delta\}$. *We also define the section* $\Sigma = \{\boldsymbol{K} = (x, y, I, \phi) \in \partial U : \phi_p = 0\}$.

Finally, consider general points $\boldsymbol{K} = (x, y, I, \phi) \in U$ outside the local stable and unstable manifolds $W^{\mathrm{s,u}}_{\mathrm{loc}}(\Lambda)$, which implies that $xy \neq 0$. Inside U, the dynamics are governed by the differential equations

$$\dot{x} = \lambda x, \quad \dot{y} = -\lambda y, \text{ and } \dot{\phi} = \nu.$$

The corresponding flow is given by $\Phi_t(\boldsymbol{K}) = \left(\mathrm{e}^{\lambda t}x, \mathrm{e}^{-\lambda t}y, I, \phi + t\nu\right)$, which confirms that both $I_{\mathrm{s}} = xy$ and I are constants of motion. For $s = xy \neq 0$, we will show that the domain U is stratified into several zones, depending of the number of times the trajectories intersect the section Σ. To avoid tracking sign combinations throughout, we first restrict our explicit formulas to the first quadrant $x > 0, y > 0$, and later adapt equations (4.9) to the remaining three quadrants.

The trajectory $\Phi_t(\boldsymbol{K})$ enters and exits U by connecting the incoming and outgoing boundary sections (see Figure 1): it starts at a point $\boldsymbol{K}_+ = (s/\delta, \delta, I, \phi_+) \in \Sigma_+$, passes through $\boldsymbol{K}$, and ends at $\boldsymbol{K}_- = (\delta, s/\delta, I, \phi_-) \in \Sigma_-$. The entry and exit angles are linked by $\phi_- = \phi_+ + T_{\mathrm{int}}\nu$, where $\nu = \nu(s, I)$. The *internal transit time* T_{int} within U, associated with the Poincaré map $\Sigma_+ \to \Sigma_-$ of the Hamiltonian flow, is given by

$$T_{\mathrm{int}} = T_{\mathrm{int}}(\delta, s, I) = \frac{1}{\lambda(s, I)} \ln\frac{\delta^2}{s} = \frac{1}{\lambda^0} \ln\frac{\delta^2}{s}\left(1 + O(s, I)\right). \tag{4.6}$$

Furthermore, the starting and ending points can be expressed from $\boldsymbol{K}$ as $\boldsymbol{K}_+ = \Phi_{T_{\mathrm{int},+}}(\boldsymbol{K})$ and $\boldsymbol{K}_- = \Phi_{T_{\mathrm{int},-}}(\boldsymbol{K})$, where the partial transit times are given by $T_{\mathrm{int},+} = \dfrac{1}{\lambda}\ln\dfrac{\delta}{y}$ and $T_{\mathrm{int},-} = \dfrac{1}{\lambda}\ln\dfrac{\delta}{x}$, with $\lambda = \lambda(s, I)$. These partial times reconstruct the total transit time via $T_{\mathrm{int},+} +$

$T_{\mathrm{int},-} = T_{\mathrm{int}}$. Notably, all three time durations are independent of the angular variables ϕ_+, ϕ, and ϕ_-.

When working later with the four-dimensional reduced phase space $U_h^\Sigma = U \cap \{H = h\} \cap \Sigma$ introduced in (1.2), we will require $\boldsymbol{K}$ to be inside U_h^Σ and outside $\Sigma_\pm$. We will denote this point as $\boldsymbol{k} = (x, y, I, \phi) \in \Sigma \setminus \Sigma_\pm$, with $I_{\mathrm{p}} = f_h(0, I_{\mathrm{v}})$ and $\phi_{\mathrm{p}} = 0$. Again, the trajectory through $\boldsymbol{k}$ starts at $\boldsymbol{K}_+$ and ends at $\boldsymbol{K}_-$, but it may intersect Σ one or more times.

To quantify this phenomenon, we introduce the following.

Definition 4.2 (Transit times t_+, t_-). *Let $t_+ = t_+(s, I, \phi_{\mathrm{p},+}) > 0$ denote the first time at which the forward trajectory starting at $\boldsymbol{K}_+ = (s/\delta, \delta, I, \phi_+) \in \Sigma_+$ intersects Σ at a point $\boldsymbol{k}_+$. This corresponds to the transit time of the primary Poincaré map $\Sigma_+ \to \Sigma$. Analogously, let $-t_- = -t_-(s, I, \phi_{\mathrm{p},-}) < 0$ denote the first time at which the (backward) trajectory starting at $\boldsymbol{K}_- = (\delta, s/\delta, I, \phi_-) \in \Sigma_-$ intersects Σ at a point $\boldsymbol{k}_-$. This represents the transit time of the primary Poincaré map $\Sigma \to \Sigma_-$.*

Clearly, we have

$$0 < t_+ = \frac{2\pi - \phi_{\mathrm{p},+}}{\nu_{\mathrm{p}}} < \frac{2\pi}{\nu_{\mathrm{p}}}, \quad 0 < t_- = \frac{\phi_{\mathrm{p},-}}{\nu_{\mathrm{p}}} < \frac{2\pi}{\nu_{\mathrm{p}}}, \quad \text{for } \phi_{\mathrm{p},\pm} \in (0, 2\pi), \tag{4.7}$$

where $\nu_{\mathrm{p}} = \nu_{\mathrm{p}}(s, I)$ is given in (4.5).

The trajectory starting at $\boldsymbol{K}_+ \in \Sigma_+$ and ending at $\boldsymbol{K}_- \in \Sigma_-$ intersects $\Sigma \setminus \Sigma_\pm$ exactly once if and only if the following *one-cut condition* holds

$$t_+ < T_{\mathrm{int}} \leq t_+ + \frac{2\pi}{\nu_p}, \tag{4.8}$$

where T_{int} is the internal transit time (4.6).

Indeed, the inequality $t_+ < T_{\mathrm{int}}$ ensures that the first intersection occurs before T_{int}, whereas $T_{\mathrm{int}} \leq t_+ + \dfrac{2\pi}{\nu_p}$ guarantees that the second intersection takes place after T_{int}. Under this condition, it also follows that $\boldsymbol{k}_+ = \boldsymbol{k} = \boldsymbol{k}_-$ and $t_+ + t_- = T_{\mathrm{int}}$.

Substituting the expression for T_{int} given in (4.6), the one-cut condition (4.8) is equivalent to

$$\mathrm{e}^{-2\pi\lambda/\nu_{\mathrm{p}}} < \frac{s}{\delta^2}\,\mathrm{e}^{\lambda t_+} \leq 1, \tag{4.9}$$

with t_+ given in (4.7) and $\lambda = \lambda(s, I)$, $\nu_{\mathrm{p}} = \nu_{\mathrm{p}}(s, I)$ in (4.4-4.5).

Remark 4.3. Although condition (4.9) for a single intersection with $\Sigma \setminus \Sigma_\pm$ might seem restrictive, it is easily satisfied in practice. For instance, when λ and ν_{p} are of the same order of magnitude ($\lambda/\nu_{\mathrm{p}} = O(1)$), we find that $\exp(-2\pi\lambda/\nu_{\mathrm{p}}) = O(10^{-3})$. Thus, across almost the entire square $|x|, |y| \leq \delta$, trajectories inside U cross $\Sigma \setminus \Sigma_\pm$ exactly once. Trajectories experiencing multiple intersections are confined to a tiny region extremely close to the invariant axes $x = 0$ and $y = 0$.

For trajectories with multiple intersections–specifically, $\ell \geq 1$ additional crossings (yielding $\ell + 1 \geq 2$ intersections in total)–we shift t_+ in (4.9) to $t_+ + \dfrac{2\pi\ell}{\nu_{\mathrm{p}}}$. This adjustment accounts for the fact that the transit time of the primary Poincaré map $\Sigma \to \Sigma$ is $\dfrac{2\pi}{\nu_{\mathrm{p}}}$. Consequently, the $(\ell + 1)$-*cuts condition* becomes

$$\mathrm{e}^{-2\pi\lambda/\nu_{\mathrm{p}}}\,\mathrm{e}^{-2\pi\ell\lambda/\nu_{\mathrm{p}}} < \frac{s}{\delta^2}\,\mathrm{e}^{\lambda t_+} \leq \mathrm{e}^{-2\pi\ell\lambda/\nu_{\mathrm{p}}}.$$

To fully characterize the square $|x|, |y| \leq \delta$ away from the invariant manifolds $x = 0$ and $y = 0$, there remains a 0-cut zone in the (x, y) plane. This zone corresponds to trajectories

where $t_+ \geq T_{\text{int}}$ or, equivalently, when the *0-cuts condition* holds:

$$e^{-\lambda t_+} < \frac{s}{\delta^2} \leq 1.$$

5. Transition map in BNF coordinates. Let U be the BNF domain given by Equation (4.2), with incoming/outgoing boundary sections $\Sigma_\pm \in \partial U$. We think of int U as the *interior* domain, containing the NHIM Λ, and out U as the *exterior* domain, containing the homoclinic channel Γ.

This section explains how the transition map is computed in a non-perturbative setting, using Equation (2.4). In that equation, $\Phi_{T_+} \circ \Phi_{T_-}$ corresponds to homoclinic orbit segments from the outgoing boundary section Σ_- to the incoming boundary section Σ_+, while the local wave maps $\Omega_\pm^{\Gamma_\pm}$ become simply standard projections in BNF coordinates. After that, the dynamics is restricted to a 4-dimensional *reduced phase space* U_h^Σ by fixing the value of the energy and using a Poincaré section. The dynamics is described by the first return map $\mathcal{F}$ of the Hamiltonian flow. We derive the *reduced transition map* of $\mathcal{F}$ from the transition map of the flow.

5.1. Transition map. We recall how the homoclinic orbits are computed following [22]. Let $\boldsymbol{Z}_- \in W^u(\Lambda)$ and $\boldsymbol{Z}_+ \in W^s(\Lambda)$ be two arbitrary points in the outgoing (resp. incoming) boundary section of the BNF domain U, with coordinates

$$\boldsymbol{Z}_- = (\delta, 0, I_-, \phi_-) \in \Sigma_- \subset \partial U$$
$$\boldsymbol{Z}_+ = (0, \delta, I_+, \phi_+) \in \Sigma_+ \subset \partial U.$$

(For simplicity, we consider the case $x = y = \delta > 0$, but x or $y = -\delta < 0$ is analogous). The variables (I_-, ϕ_-) and (I_+, ϕ_+) determine $\boldsymbol{Z}_-$ and $\boldsymbol{Z}_+$, and they are parameters to be found during the procedure.

Numerically integrate the trajectory starting at $\boldsymbol{Z}_-$ forward in time until it intersects some exterior section $\mathscr{S}$ at a point $\mathcal{K}_- = \Phi_{T_-}(\boldsymbol{Z}_-)$. Similarly, integrate the trajectory starting at $\boldsymbol{Z}_+$ backward in time until it intersects $\mathscr{S}$ at a point $\mathcal{K}_+ = \Phi_{T_+}(\boldsymbol{Z}_+)$. To find a homoclinic, iteratively correct (I_-, ϕ_-) and (I_+, ϕ_+) using a Newton-like method, until $\mathcal{K}_+ = \mathcal{K}_- = \mathcal{K}$.

Notice that $[\boldsymbol{Z}_-, \boldsymbol{Z}_+]$ is a finite time homoclinic orbit segment of length $T_{\text{ext}} = T_- + T_+$. The exterior Poincaré map $P_{\text{ext}} = \Phi_{T_+} \circ \Phi_{T_-}$ takes Z_- to Z_+. The times $T_\pm = T_\pm(\mathcal{K})$ are continuous functions on Γ. (See Remark 2.3).

Remark 5.1. These type of homoclinic intersections at the "first cut" of the asymptotic manifolds with $\mathscr{S}$ are usually called *primary* or *one-round homoclinics*.

Remark 5.2. In practice, to determine the homoclinic channels, one can compute all the (primary) homoclinics from Λ to Λ, and then identify continuous families of homoclinics with the property that the restrictions $\Omega_\pm^\Gamma$ are diffeomorphisms onto their images. In [22], we illustrate this computation in the case of the SR3BP around the equilibrium point L_1, with small enough energy. We show that there are two different homoclinic channels Γ_1, Γ_2. By suitably restricting Γ_1, Γ_2, the associated scattering maps $\mathcal{S}_1, \mathcal{S}_2$ are defined in a common domain.

Assume that $\mathcal{K}$ belongs to a homoclinic channel Γ as defined in Section 2. By construction, $\boldsymbol{Z}_+ \in W^s(\boldsymbol{X}_+)$, where $\boldsymbol{X}_+ = (0, 0, I_+, \phi_+) \in \Lambda$. Indeed, using the BNF equations (4.3), where $\lambda = \lambda(0, I_+) > 0$ and $\nu = \nu(0, I_+)$ are given by equations (4.4–4.5), the forward flows read

$$\Phi_t(\boldsymbol{Z}_+) = \big(0,\, e^{-t\lambda}\delta, I_+, \phi_+ + t\nu\big),$$
$$\Phi_t(\boldsymbol{X}_+) = \big(0, 0, I_+, \phi_+ + t\nu\big).$$

Consequently, their difference satisfies

$$\Phi_t(\boldsymbol{Z}_+) - \Phi_t(\boldsymbol{X}_+) = \big(0,\, e^{-t\lambda}\delta, \mathbf{0}, \mathbf{0}\big) \longrightarrow \mathbf{0} \quad \text{as } t \to \infty.$$

Thus, in BNF coordinates, the wave map $\Omega_+^{\Gamma_+}$ is simply the standard projection onto Λ:

$$\boldsymbol{Z}_+ = (0, \delta, I_+, \phi_+) \in W^{\mathrm{s}}_{\mathrm{loc}}(\Lambda) \mapsto \boldsymbol{X}_+ = (0, 0, I_+, \phi_+) \in \Lambda.$$

Remark 5.3. $\boldsymbol{Z}_+$ "synchronizes in the far future" with $\boldsymbol{X}_+$. The wave map $\boldsymbol{Z}_+ \mapsto \boldsymbol{X}_+$ maps a point to its future synchronized state on the NHIM. The stable manifold $W^{\mathrm{s}}(\boldsymbol{X}_+)$ is also referred to as the *stable isochrone manifold* of $\boldsymbol{X}_+$.

Analogously, $\boldsymbol{Z}_- \in W^{\mathrm{u}}(\boldsymbol{X}_-)$ where $\boldsymbol{X}_- = (0, 0, I_-, \phi_-) \in \Lambda$. Thus, in BNF coordinates, the wave map $\Omega_-^{\Gamma_-}$ is simply the standard projection onto Λ:

$$\boldsymbol{Z}_- = (\delta, 0, I_-, \phi_-) \in W^{\mathrm{u}}_{\mathrm{loc}}(\Lambda) \mapsto \boldsymbol{X}_- = (0, 0, I_-, \phi_-) \in \Lambda.$$

Finally, the transition map $\mathcal{T}\colon\ \Lambda \to \Lambda$, $\boldsymbol{X}_+ = \mathcal{T}(\boldsymbol{X}_-)$ is given by the composition (2.4) of the exterior Poincaré map $P_{\mathrm{ext}} = \Phi_{T_+} \circ \Phi_{T_-}$ with the local wave maps $\Omega_\pm^{\Gamma_\pm}$:

$$\boldsymbol{X}_- = (0, 0, I_-, \phi_-) \mapsto \boldsymbol{Z}_- = (\delta, 0, I_-, \phi_-) \mapsto \boldsymbol{Z}_+ = (0, \delta, I_+, \phi_+) \mapsto \boldsymbol{X}_+ = (0, 0, I_+, \phi_+),$$

or simply

$$\boldsymbol{X}_- = (I_-, \phi_-) \mapsto \boldsymbol{X}_+ = (I_+, \phi_+).$$

Remark 5.4. In Definition 2.1 the scattering map depends only on the choice of the homoclinic channel Γ, while in Definition 2.2 the transition map additionally depends on the times $T_\pm$, which in turn depend on the sections $\Sigma_\pm$. On the one hand, the definition of scattering map is conceptually simpler than the transition map. On the other hand, the numerical computation of the transition map is more straightforward. To obtain the scattering map, one would first compute the transition map $\boldsymbol{X}_- \mapsto \boldsymbol{X}_+$, and then derive the scattering map using Equation (2.3).

Remark 5.5. Note again that in formula (2.3) relating the scattering map and the transition map, the flow $\Phi_{T_\pm}$ is only needed on the NHIM Λ and therefore only involves translations for the angles $\phi = (\phi_{\mathrm{p}}, \phi_{\mathrm{v}})$ in the BNF variables, that is, the *inner flow* inside the NHIM Λ where the actions $I_{\mathrm{s}} = 0$, $I = (I_{\mathrm{p}}, I_{\mathrm{v}})$ remain constant.

5.2. Reduced transition map. Inside the BNF domain U, we can pass from the flow to a discrete-time dynamical system $\mathcal{F}$, given by the first return map to a Poincaré section Σ. The map $\mathcal{F}$ inherits an associated NHIM Λ_h^Σ that is easily obtained from Λ. Moreover, we derive the transition map $\tau\colon \Lambda_c^\Sigma \to \Lambda_c^\Sigma$ of $\mathcal{F}$ from the transition map $\mathcal{T}\colon \Lambda \to \Lambda$ of Φ_t. Since τ is lower-dimensional, we refer to it as the *reduced transition map*. In what follows, we derive the expressions of these transition maps in BNF coordinates.

The original Hamiltonian system has a conserved quantity, the energy H, which is the energy $\mathcal{Z}$ of the BNF when the remainder is neglected. For a fixed energy $H \circ \Psi = h > h^0$, the action I_{p} can be given as an implicit function of $I_{\mathrm{s}}, I_{\mathrm{v}}, h$: $I_{\mathrm{p}} = (h - h^0 - I_{\mathrm{s}} - \nu_{\mathrm{v}}^0 I_{\mathrm{v}})/\nu_{\mathrm{p}}^0 + O_2(I_{\mathrm{s}}, I_{\mathrm{v}}) =: f_h(I_{\mathrm{s}}, I_{\mathrm{v}})$. The corresponding 3-dimensional NHIM on the level of energy $H = h$ is given by $\Lambda_h = \Lambda \cap \{H \circ \Psi = h\}$ and is parameterized by the variables $\phi_{\mathrm{p}}, \phi_{\mathrm{v}}, I_{\mathrm{v}}$. Taking it one step further, we can consider the Poincaré section

$$\Sigma \coloneqq \{(x, y, I, \phi) \in U \ :\ \phi_{\mathrm{p}} = 0\},$$

which is a global section within U, and denote

$$\Lambda_h^\Sigma = \Lambda_h \cap \Sigma = \{\boldsymbol{x} = (0, 0, I, \phi) : \phi_{\mathrm{p}} = 0, I_{\mathrm{p}} = f_h(0, I_{\mathrm{v}}), I_{\mathrm{v}} \in [0, r], \phi_{\mathrm{v}} \in \mathbb{T}\}$$

the associated 2-dimensional NHIM of the return map, which is parameterized by the variables $\phi_{\mathrm{v}}, I_{\mathrm{v}}$.

Next, we compute the 2-dimensional reduced transition map $\tau\colon \Lambda_h^\Sigma \to \Lambda_h^\Sigma$ associated to $\mathcal{F}$, which is exact symplectic (see Section 2). Recall from the above construction that $\boldsymbol{Z}_\pm \in \Sigma_\pm$

satisfy $\boldsymbol{Z}_\pm \in W^{\mathrm{s/u}}(\boldsymbol{X}_\pm)$, where $\boldsymbol{X}_\pm = (0,0,I_\pm,\phi_\pm) \in \Lambda$. Let $\boldsymbol{T}_\pm = T_\pm + t_\pm \geq T_\pm$ be the first times such that the forward and backward trajectories of $\mathcal{K} \in \Gamma$ reach the section $\Sigma = \{\phi_{\mathrm{p}} = 0\}$ inside U. In other words, $t_+, t_- > 0$ are the transit times of $\boldsymbol{Z}_\pm \in \Sigma_\pm$ to the Poincaré section Σ. (See Definition 4.2).

Define new points

$$\begin{aligned} \boldsymbol{z}_+ &= \Phi_{t_+}(\boldsymbol{Z}_+) = \big(0,\rho_+,I_+,\widetilde{\phi}_+\big) := \big(0,\, \mathrm{e}^{-t_+\lambda}\delta, I_+, \phi_+ + t_+\nu\big) \in \Sigma, \\ \boldsymbol{z}_- &= \Phi_{-t_-}(\boldsymbol{Z}_-) = \big(\rho_-,0,I_-,\widetilde{\phi}_-\big) := \big(\mathrm{e}^{t_-\lambda}\delta, 0, I_-, \phi_- - t_-\nu\big) \in \Sigma. \end{aligned}$$

Notice that $\boldsymbol{z}_\pm$ belong to the reduced phase space U_h^Σ, that is, their planar angle and action satisfy $\widetilde{\phi}_{\mathrm{p}} = 0$, $I_{\mathrm{p}} = f_h(I_{\mathrm{s}}, I_{\mathrm{v}})$. See Figure 1.

Due to the conjugacy of invariant fibers $W^{\mathrm{s/u}}(x)$ by the flow, we have $\boldsymbol{z}_+ \in W^{\mathrm{s}}(\boldsymbol{x}_+)$ and $\boldsymbol{z}_- \in W^{\mathrm{u}}(\boldsymbol{x}_-)$, where

$$\begin{aligned} \boldsymbol{x}_+ &= \Phi_{t_+}(\boldsymbol{X}_+) = \big(0,0,I_+,\widetilde{\phi}_+\big) = \big(0,0,I_+,\phi_+ + t_+\nu\big) \in \Lambda_h^\Sigma, \\ \boldsymbol{x}_- &= \Phi_{-t_-}(\boldsymbol{X}_-) = \big(0,0,I_-,\widetilde{\phi}_-\big) = \big(0,0,I_-,\phi_- - t_-\nu\big) \in \Lambda_h^\Sigma, \end{aligned}$$

that is, their planar angle and action satisfy $\phi_{\mathrm{p}} = 0, I_{\mathrm{p}} = f_h(0, I_{\mathrm{v}})$.

Thus, for the discrete system, in BNF coordinates, the wave maps $\Omega_\pm$ are also the standard projection onto Λ_h^Σ, and the reduced transition map $\tau\colon \Lambda_h^\Sigma \to \Lambda_h^\Sigma$, $\boldsymbol{x}_+ = \tau(\boldsymbol{x}_-)$ is given by

$$\boldsymbol{x}_- = (I_{\mathrm{v},-}, \widetilde{\phi}_{\mathrm{v},-}) \mapsto \boldsymbol{x}_+ = (I_{\mathrm{v},+}, \widetilde{\phi}_{\mathrm{v},+}).$$

Remark 5.6. The reduced transition map depends on the choice of Σ, a global section within U, which in turn uniquely determines the times $t_\pm$. These times must satisfy $\phi_{\mathrm{p}_\pm} \equiv 0 \pmod{2\pi}$, so there is an infinite but discrete set of them. However, any two reduced transition maps $\tau = \tau(\boldsymbol{T}_\pm)$ and $\tau' = \tau'\left(\boldsymbol{T}'_\pm\right)$ are related in the following way

$$\tau = \Phi_{-(\boldsymbol{T}'_+ - \boldsymbol{T}_+)} \circ \tau' \circ \Phi_{-(\boldsymbol{T}'_- - \boldsymbol{T}_-)}.$$

If τ maps the point $\boldsymbol{x}_- = (I_{\mathrm{v},-}, \phi_{\mathrm{v},-})$ to $\boldsymbol{x}_+ = (I_{\mathrm{v},+}, \phi_{\mathrm{v},+})$, where, for simplicity of notation, we only write the components $(I_{\mathrm{v}}, \phi_{\mathrm{v}})$ of $\boldsymbol{x}_\pm$, which are the signicant ones, then τ' maps the point $\boldsymbol{x}'_- = \big(I'_{\mathrm{v},-}, \phi'_{\mathrm{v},-}\big) = \big(I_{\mathrm{v},-}, \phi_{\mathrm{v},-} - \left(\boldsymbol{T}'_- - \boldsymbol{T}_-\right)\nu_{\mathrm{v}}\left(I_{\mathrm{v},-}\right)\big)$ to $\boldsymbol{x}'_+ = \big(I'_{\mathrm{v},+}, \phi'_{\mathrm{v},+}\big) = \big(I_{\mathrm{v},+}, \phi_{\mathrm{v},+} + \left(\boldsymbol{T}'_+ - \boldsymbol{T}_+\right)\nu_{\mathrm{v}}\left(I_{\mathrm{v},+}\right)\big)$. Thus, both pre-images $\boldsymbol{x}_-$ and $\boldsymbol{x}'_-$ have the same action $I_{\mathrm{v},-}$ but their angle differs by a shift. Similarly, both images $\boldsymbol{x}_+$ and $\boldsymbol{x}'_+$ have the same action $I_{\mathrm{v},+}$ but their angle differs by a shift.

Notation warning: When clear from the context, the 'reduced transition map' and 'reduced scattering map' are abbreviated just as 'transition map' and 'scattering map'.

6. Analytical shadowing.

In this section, we provide the proof of Theorem 3.1. We proceed in a constructive and direct way.

6.1. Proof of Theorem 3.1.

Let $(\boldsymbol{x}_i)_{i=1}^N$ be a guiding orbit of the iterated function system (IFS) defined on the reduced NHIM Λ_h^Σ (1.3) generated by $L \geq 1$ transition maps $\{\tau_1, \ldots, \tau_L\}$, expressed in BNF coordinates (1.1). Let $(\boldsymbol{Z}_i^-, \boldsymbol{Z}_{i+1}^+)_{i=1}^{N-1}$ be the pseudo-trajectory [3, Equation (3.3)], and $(\boldsymbol{z}_i^-, \boldsymbol{z}_{i+1}^+)_{i=1}^{N-1}$ be the reduced pseudo-trajectory [3, Equation (3.2)] associated with the guiding orbit.

Consider the first homoclinic segment $[\boldsymbol{Z}_1^-, \boldsymbol{Z}_2^+]$ with $\boldsymbol{Z}_1^- \in \Sigma_-$, $\boldsymbol{Z}_2^+ \in \Sigma_+$, and $\boldsymbol{Z}_2^+ = \Phi_{T_{\mathrm{ext}}^1}\left(\boldsymbol{Z}_1^-\right)$. Consider now the trajectory of any point

$$\boldsymbol{K}_1^- = \big(\delta, s_1/\delta, I^1 + \Delta I^1, \phi_-^1 + \Delta\phi_-^1\big) = \boldsymbol{Z}_1^- + \Delta\boldsymbol{Z}_1^- \in \Sigma_-$$

that is ε_-^1-close to $\boldsymbol{Z}_1^- = \big(\delta, 0, I^1, \phi_-^1\big)$, i.e., $\Delta\boldsymbol{Z}_1^- = \big(0, s_1/\delta, \Delta I^1, \Delta\phi_-^1\big)$ is small:

$$\left\|\Delta\boldsymbol{Z}_1^-\right\| = \max\left\{s_1/\delta, \left\|\Delta I^1\right\|, \left\|\Delta\phi_-^1\right\|\right\} = \varepsilon_-^1.$$

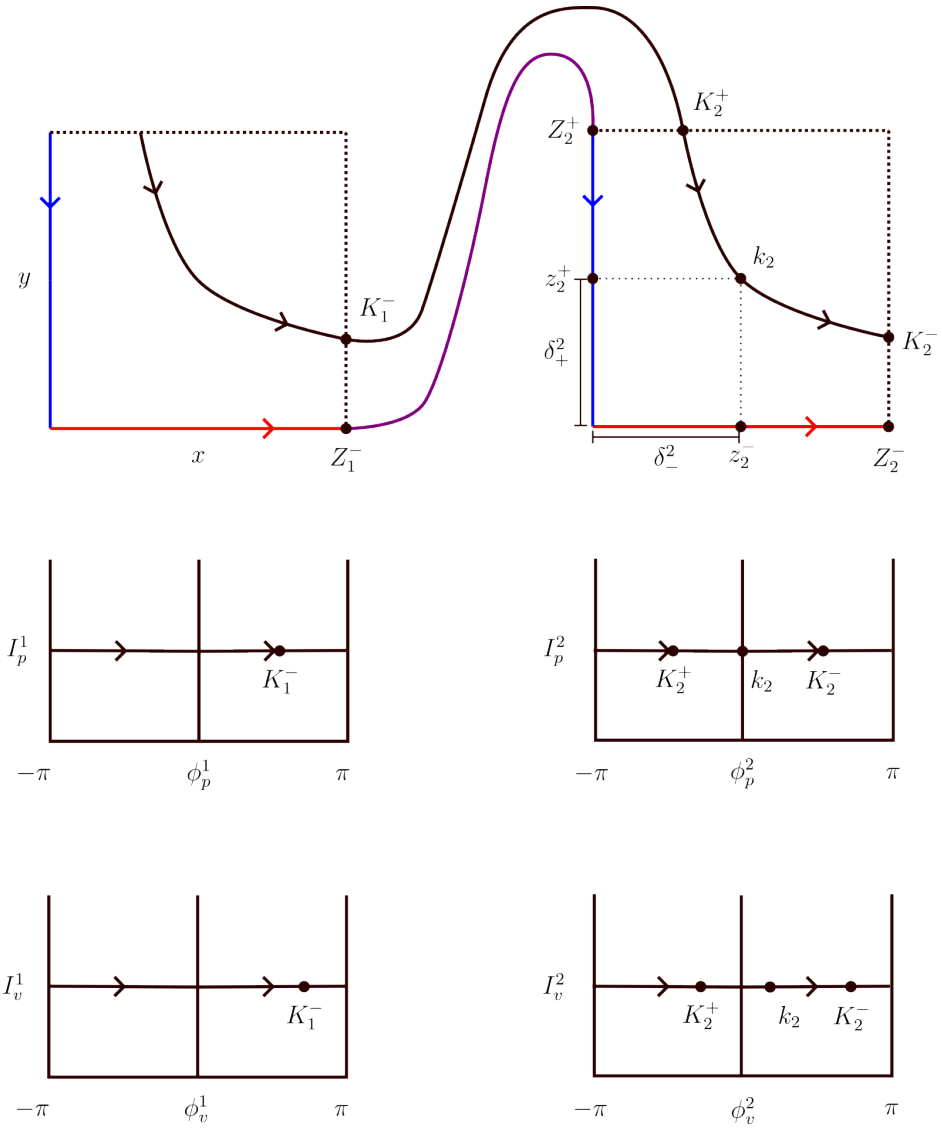


Figure 2: First step of shadowing trajectory. The trajectory through $\boldsymbol{K}_2^+$ crosses the section Σ only once at a point $\boldsymbol{k}_2$.

Outside U, if ε_-^1 is small enough, this trajectory will cut the incoming boundary section Σ_+ at a point

$$\boldsymbol{K}_2^+ = P_{\text{ext}}(\boldsymbol{K}_1^-) = \left(s_2/\delta, \delta, \hat{I}^2 = I^2 + \Delta I^2, \hat{\phi}_+^2 = \phi_+^2 + \Delta\phi_+^2\right) = \boldsymbol{Z}_2^+ + \Delta\boldsymbol{Z}_2^+ \in \Sigma_+,$$

where $P_{\text{ext}} : \Sigma_- \to \Sigma_+$ is the Poincaré map of the Hamiltonian flow associated to the homoclinic segment $[\boldsymbol{Z}_1^-, \boldsymbol{Z}_+^2]$. $\boldsymbol{K}_2^+$ is ε_+^2-close to $\boldsymbol{Z}_+^2 = \left(0, \delta, I^2, \phi_+^2\right)$, i.e., $\Delta\boldsymbol{Z}_2^+ = \left(s_2/\delta, 0, \Delta I^2, \Delta\phi_+^2\right)$ satisfies

$$\left\|\Delta\boldsymbol{Z}_2^+\right\| = \max\left\{s_2/\delta, \left\|\Delta I^2\right\|, \left\|\Delta\phi_+^2\right\|\right\} = \varepsilon_+^2,$$

see Figure 6.

Denoting the uniform log-scale bound χ as

$$\mathrm{e}^{\chi} := \max\left\{\max_{\boldsymbol{Z}_- \in \Sigma_-} \|DP_{\text{ext}}(\boldsymbol{Z}_-)\|, \max_{\boldsymbol{Z}_+ \in \Sigma_+} \left\|DP_{\text{ext}}^{-1}(\boldsymbol{Z}_+)\right\|\right\},$$

it follows from the Mean Value Inequality that the variations $\Delta\boldsymbol{Z}_1^-$, $\Delta\boldsymbol{Z}_2^+$ satisfy the uniform

bi-Lipschitz bound

$$\mathrm{e}^{-\chi}\|\Delta \boldsymbol{Z}_1^-\| \le \|\Delta \boldsymbol{Z}_2^+\| \le \mathrm{e}^{\chi}\|\Delta \boldsymbol{Z}_1^-\|, \tag{6.1}$$

so $\varepsilon_+ \le \mathrm{e}^{\chi}\varepsilon_-$.

Continuing inside U, the trajectory of $\boldsymbol{K}_2^+$, with $0 < s_2 < \delta^2$, is given by

$$\Phi_t\left(\boldsymbol{K}_2^+\right) = \left(\mathrm{e}^{t\lambda}s_2/\delta,\, \mathrm{e}^{-t\lambda}\delta, \hat{I}^2, \hat{\phi}_+^2 + t\,\nu\right).$$

where λ and ν are evaluated at $\left(s_2, \hat{I}^2\right)$ and are given in (4.4–4.5),

We now extend $\Phi_t\left(\boldsymbol{K}_2^+\right)$ until it reaches a point

$$\boldsymbol{K}_2^- = \left(\delta, s_2/\delta, \hat{I}^2, \hat{\phi}_+^2 + T_{\mathrm{int}}^2\,\nu\right) = \boldsymbol{Z}_2^- + \Delta\boldsymbol{Z}_2^- \in \Sigma_-,$$

with $\boldsymbol{Z}_2^- = \left(\delta, 0, I^2, \phi_-^2\right) \in \Sigma_-$ and $\Delta\boldsymbol{Z}_2^- = \left(0, s_2/\delta, \Delta I^2, \left(\phi_+^2 + T_{\mathrm{int}}^2\,\nu - \phi_-^2\right) + \Delta\phi_+^2\right)$, where we have used the dynamical invariance of $I_{\mathrm{s}} = xy = s_2$ and I, and the *internal transit time* (4.6)

$$T_{\mathrm{int}}^2 = T_{\mathrm{int}}^2(\delta, s_2, \hat{I}^2) = \frac{\ln\left(\delta^2/s_2\right)}{\lambda\left(s_2, \hat{I}^2\right)} = \frac{1}{\lambda^0}\ln\frac{\delta^2}{s_2}\left(1 + O(s_2, \hat{I}^2)\right).$$

We can exploit the dependence of T_{int}^2 with respect to the parameter s_2 to ensure that $\phi_+^2 + T_{\mathrm{int}}^2\,\nu - \phi_-^2$ is small. Equivalently, this ensures that $\phi_+^2 + T_{\mathrm{int}}^2\,\nu$ remains close to the angular component $\phi_-^2 \in \mathbb{T}^2$ of the subsequent point $\boldsymbol{Z}_2^- = \left(\delta, 0, I^2, \phi_-^2\right) \in \Sigma_-$, which belongs to the next homoclinic segment $\left[\boldsymbol{Z}_2^-, \boldsymbol{Z}_3^+\right]$.

Notice that $\boldsymbol{Z}_2^+$ and $\boldsymbol{Z}_2^-$ are linked because their saddle components permute from $(0, \delta)$ to $(\delta, 0)$. Meanwhile, their center components follow a BNF trajectory from (I^2, ϕ_+^2) to $\left(I^2, \phi_-^2\right)$, satisfying $\phi_-^2 = \phi_+^2 + \hat{T}_{\mathrm{int}}^2\nu(0, I^2)$. When the trajectory through $\boldsymbol{K}_2^+$ crosses the section Σ *only once* at a point $\boldsymbol{k}_2 = \left(\delta_+^2, \delta_-^2, I^2, \phi^2\right)$, with $\delta_+^2\,\delta_-^2 = s_2$ and $\phi_{\mathrm{p}}^2 = 0$, that is, it is contained in the one-cut zone (4.9), it spends a time t_+^2 during the transition $\Sigma_+ \to \Sigma$ (the primary Poincaré map), and a time t_-^2 during $\Sigma \to \Sigma_-$. Consequently, the total internal transition time $\hat{T}_{\mathrm{int}}^2$ is given by

$$\hat{T}_{\mathrm{int}}^2 = t_+^2 + t_-^2 = \frac{1}{\lambda(0, I^2)}\ln\frac{\delta^2}{s_2} = \frac{1}{\lambda^0}\ln\frac{\delta^2}{s_2}\left(1 + O(I^2)\right).$$

Inside the one-cut zone (4.9), the angular difference simplifies to:

$$\begin{aligned}
\phi_+^2 + T_{\mathrm{int}}^2\,\nu - \phi_-^2 &= \phi_+^2 + \hat{T}_{\mathrm{int}}^2\,\nu(0, I^2) - \phi_-^2 + T_{\mathrm{int}}^2\,\nu - \hat{T}_{\mathrm{int}}^2\,\nu(0, I^2) \\
&= T_{\mathrm{int}}^2\,\nu\left(s_2, \hat{I}^2\right) - \hat{T}_{\mathrm{int}}^2\,\nu(0, I^2) \\
&= \ln\frac{\delta^2}{s_2}\left(\frac{\nu\left(s_2, \hat{I}^2\right)}{\lambda\left(s_2, \hat{I}^2\right)} - \frac{\nu(0, I^2)}{\lambda(0, I^2)}\right) = \ln\frac{\delta^2}{s_2}\,O\left(s_2, \Delta I^2\right),
\end{aligned}$$

which yields

$$\Delta\boldsymbol{Z}_2^- = \left(0, s_2/\delta, \Delta I^2, \Delta\phi_+^2 + \ln\frac{\delta^2}{s_2}\,O\left(s_2, \Delta I^2\right)\right).$$

Inside the one-cut zone (4.9) we have that $\ln\dfrac{\delta^2}{s} < \dfrac{4\pi\lambda}{\nu_{\mathrm{p}}}$. Thus, there exists a constant $c > 0$ such that

$$\|\Delta\boldsymbol{Z}_2^-\| \le c\|\Delta\boldsymbol{Z}_2^+\|,$$

which finally leads to

$$\|\Delta\boldsymbol{Z}_2^-\| \le C\|\Delta\boldsymbol{Z}_1^-\|$$

where $C = \mathrm{e}^{\chi} c$.

Iterating this process along the guiding orbit, we finally obtain

$$\left\|\boldsymbol{K}_i^- - \boldsymbol{Z}_i^-\right\| = \left\|\Delta \boldsymbol{Z}_i^-\right\| \leq C^{i-1}\left\|\Delta \boldsymbol{Z}_1^-\right\|, \quad i = 2, \ldots, N.$$

Notice that we only need for the recursion that successive $\boldsymbol{K}_i^- \in \Sigma_-$, so choosing $\boldsymbol{K}_1^- - \boldsymbol{Z}_1^- = \Delta \boldsymbol{Z}_1^- = \left(0, s_1/\delta, \Delta I^1, \Delta \phi_-^1\right)$ small enough such that $C^{N-1}\left\|\Delta \boldsymbol{Z}_1^-\right\| < \delta$, we obtain a true trajectory $\Phi(t)$ of the system that satisfies $\left\|\Phi(t_i) - \boldsymbol{Z}_i^-\right\| < \delta$ for some times $0 < t_1 < \cdots < t_N$.

It remains to check that the trajectories through successive $\boldsymbol{K}_i^-$ cross Σ exactly once, so that they are in the one-cut zone (4.9), that is,

$$\mathrm{e}^{-2\pi\lambda/\nu_{\mathrm{p}}} < \frac{s_i}{\delta^2}\,\mathrm{e}^{\lambda t_{+,i}} \leq 1, \tag{6.2}$$

with $0 < t_{+,i} = \dfrac{2\pi - \phi_{+,\mathrm{p}}^i}{\nu_{\mathrm{p}}} < \dfrac{2\pi}{\nu_{\mathrm{p}}}$ as in (4.7) and $\lambda = \lambda(s_i, I^i)$, $\nu_{\mathrm{p}} = \nu_{\mathrm{p}}(s_i, I^i)$ as in (4.4-4.5).

By the bounds (6.1) and (4.7) , we just need to have

$$\mathrm{e}^{-2\pi\lambda/\nu_{\mathrm{p}}} < \mathrm{e}^{-(i-1)\chi}\frac{s_1}{\delta^2}\,\mathrm{e}^{-2\pi\lambda/\nu_{\mathrm{p}}} < \mathrm{e}^{(i-1)\chi}\frac{s_1}{\delta^2}\,\mathrm{e}^{2\pi\lambda/\nu_{\mathrm{p}}} \leq 1, \quad i = 1, \ldots, N,$$

which can be written as

$$\mathrm{e}^{(i-1)\chi} < \frac{s_1}{\delta^2}, \qquad \frac{s_1}{\delta^2}\,\mathrm{e}^{2\pi\lambda/\nu_{\mathrm{p}}} \leq \mathrm{e}^{-(i-1)\chi},$$

and is implied by the inequalities that take place for $i = N$

$$\mathrm{e}^{(N-1)\chi} < \frac{s_1}{\delta^2} < \mathrm{e}^{-(N-1)\chi}\,\mathrm{e}^{-2\pi\lambda/\nu_{\mathrm{p}}}. \tag{6.3}$$

For the bounds (6.3) to be satisfied, we need a left hand side smaller than the right hand side, that is

$$(N-1)\chi < \pi\lambda/\nu_{\mathrm{p}}, \tag{6.4}$$

which will be called the *homecoming condition*.

Under this condition, choosing any s_1 satisfying (6.3), for instance $s_1 = \delta^2 \exp\left(-\pi\lambda/\nu_{\mathrm{p}}\right)$ or close enough, the bounds (6.2) are satisfied, and the sequence $\boldsymbol{K}_i^{\pm}$ is well defined.

Furthermore, since each point $\boldsymbol{k}_i = \left(\delta_-^i, \delta_+^i, I^i, \phi^i\right) \in \Sigma$, where $\delta_+^i\,\delta_-^i = s_i$ and $\phi_{\mathrm{p}}^i = 0$, belongs to the trajectory that joins $\boldsymbol{K}_i^+$ to $\boldsymbol{K}_i^-$, it is also clear that $\|\Phi(t_i) - \boldsymbol{k}_i\| < \delta$ holds for *any* time of the trajectory joining $\boldsymbol{K}_i^+$ to $\boldsymbol{K}_i^-$, in particular for the time associated to the point $\boldsymbol{k}_i$. For the total drift trajectory we can choose $t_1 = \boldsymbol{T}_1$, and at the step i the accumulated time can be thus chosen as $t_i = \boldsymbol{T}_1 + \cdots + \boldsymbol{T}_i$.

7. Topological shadowing.

In this section we provide the proofs of Lemma 2.6 and Theorem 3.2.

7.1. Proof of Lemma 2.6.

Construction of a sequence of balls in Λ. Let τ_i be a transition map on Λ, for some corresponding $m_i, n_i > 0$. If $B_r^c(\boldsymbol{x})$ is a ball of radius r centered at $\boldsymbol{x} \in \Lambda$, then we define the inner and outer radii

$$\begin{aligned} r_{\min}^i(\boldsymbol{x}, r) &= \sup\{\rho > 0 \,|\, B_\rho^c(\tau_i(\boldsymbol{x})) \subseteq \tau_i(B_r^c(\boldsymbol{x}))\} \\ r_{\max}^i(\boldsymbol{x}, r) &= \inf\{\rho > 0 \,|\, \tau_i(B_r^c(\boldsymbol{x})) \subseteq B_\rho^c(\tau_i(\boldsymbol{x}))\}. \end{aligned}$$

Due to the expansion $\tau_i(\boldsymbol{x} + h) = \tau_i(\boldsymbol{x}) + D\tau_i(\boldsymbol{x})h + O(h^2)$ we have that

$$\begin{aligned} r_{\min}^i(\boldsymbol{x}, r) &= s_{\min}^i(D\tau_i(\boldsymbol{x}))r + O(r^2) \\ r_{\max}^i(\boldsymbol{x}, r) &= s_{\max}^i(D\tau_i(\boldsymbol{x}))r + O(r^2) \end{aligned}$$

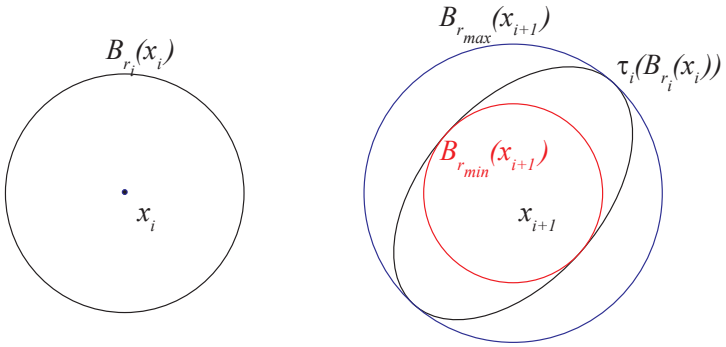


Figure 3: Sequence of balls in Λ.

.

where $s^i_{\min}(\tau_i(\boldsymbol{x}))$ and $s^i_{\max}(\tau_i(\boldsymbol{x}))$ are the smallest and the largest singular values of $D\tau_i(\boldsymbol{x})$. Since τ_i is symplectic we have that $s^i_{\min}\cdot s^i_{\max}=1$ and $r^i_{\min}\cdot r^i_{\max}=r^2+O(r^3)$. Note that $r^i_{\min}$ and $r^i_{\max}$ depend on $\boldsymbol{x}$, r and τ_i, and implicitly on the number of iterates $M_i=n_i+m_i$.

As Λ is compact and the collection of transition maps is finite, we can find two continuous functions $r_{\min}(r)$ and $r_{\max}(r)$, independent of $\boldsymbol{x}$ and i, but depending on $M_{\max}=\max\{M_1,\dots,M_{N-1}\}$, such that, for any $i\in\{1,\dots,N-1\}$, $\boldsymbol{x}\in\Lambda$ and $r>0$ we have

$$B^c_{r_{\min}(r)}(\tau_i(\boldsymbol{x}))\subseteq\tau_i(B^c_r(\boldsymbol{x}))\subseteq B^c_{r_{\max}(r)}(\tau_i(\boldsymbol{x})).$$

See Fig. 3.

We now construct inductively a finite sequence of balls in Λ as follows:

- $B^c_{r_1}(\boldsymbol{x}_1)$ for some $r_1>0$;
- $B^c_{r_{i+1}}(\boldsymbol{x}_{i+1})$ where $r_{i+1}=r_{\max}(r_i)$, for $i=1,\dots,N-1$.

By the construction, we have that

$$\tau_i(B^c_{r_i}(\boldsymbol{x}_i))\subseteq B^c_{r_{i+1}}(\boldsymbol{x}_{i+1}),\ \text{for } i=1,\dots,N-1.$$

By the continuity of the function $r_{\max}(r)$ and finiteness of the number of steps, there exists r_1 sufficiently small such that $r_1,\dots,r_N$ are all less than $\varepsilon>0$. Note that r_1 depends on $M_{\max}$.

We remark here that this construction does not involve the function $r_{\min}(r)$.

Construction of stable and unstable disks at the homoclinic intersection. Let $\Gamma_{\alpha(i)}$ be a homoclinic channel associated to $\sigma_{\alpha(i)}$.

Choose a homoclinic point $\boldsymbol{k}_i\in\Gamma_{\alpha(i)}$. Then choose a pair of transverse, 1-dimensional disks $\mathscr{D}^s_{i+1}$ around $\boldsymbol{k}_i$ in $W^s(\boldsymbol{x}_{i+1})$ and $\mathscr{D}^u_i$ around $\boldsymbol{k}_i$ in $W^u(\boldsymbol{x}_i)$, respectively.

By the Lambda Lemma, $\mathcal{F}^{-n_i}(\mathscr{D}^s_{i+1})$ approaches a disk $B^s_{\rho_L}(x_i)$ in $W^s(\boldsymbol{x}_i)$, relative to the C^1 topology, as $n_i\to\infty$.

Also by the Lambda Lemma, $\mathcal{F}^{m_i}(\mathscr{D}^u_i)$ approaches a disk $B^u_{\rho_L}(x_{i+1})$ in $W^u(x_{i+1})$, relative to the C^1 topology, as $m_i\to\infty$.

For m_i,n_i sufficiently large (to be made precise later), we denote $\boldsymbol{z}^-_i$ the x-coordinate of $\mathcal{F}^{-n_i}(\boldsymbol{k}_i)\in\mathcal{F}^{-n_i}(\mathscr{D}^s_{i+1})\cap W^u(\Lambda)$, and $\boldsymbol{z}^+_{i+1}$ the y-coordinate of $\mathcal{F}^{m_i}(\boldsymbol{k}_i)\in\mathcal{F}^{m_i}(\mathscr{D}^u_i)\cap W^s(\Lambda)$.

Construction of correctly aligned windows in the normal form coordinates.

For the definition of correctly aligned windows and their properties see [44].

Define:

$$\begin{aligned}W^+_i&=B^u_{\rho_L}(0)\times B^s_{\rho_S}(\boldsymbol{z}^+_i)\times B^c_{r_i}(\boldsymbol{x}_i),\\ W^-_i&=B^u_{\rho_S}(\boldsymbol{z}^-_i)\times B^s_{\rho_L}(0)\times B^c_{r_i}(\boldsymbol{x}_i)\end{aligned}$$

where the superscripts u,s,c indicate that the respective balls are in the unstable, stable and center coordinates (x,y,θ) described in (2.5).

We require $\rho_L > \rho_S > 0$ to be so that

- $B^u_{\rho_L}(0) \subset \mathrm{Pr}_x[\mathcal{F}^{m_{i-1}}(\mathscr{D}^u_{i-1})]$;
- $\mathcal{F}^{m_{i-1}}(\mathscr{D}^u_{i-1})$ is a graph over x that crosses transversally each disk $\{x\} \times B^s_{\rho_S}(\boldsymbol{z}_i^+) \times B^c_{r_i}(\boldsymbol{x}_i)$ in W_i^+, for every $x \in B^u_{\rho_L}(0)$;
- $B^s_{\rho_S}(0) \subset \mathrm{Pr}_y[\mathcal{F}^{-n_i}(\mathscr{D}^s_{i+1})]$
- $\mathcal{F}^{-n_i}(\mathscr{D}^s_{i+1})$ is a graph over y that crosses transversally each disk $B^u_{\rho_S}(\boldsymbol{z}_i^-) \times \{y\} \times B^c_{r_i}(\boldsymbol{x}_i)$ in W_i^-, for every $y \in B^s_{\rho_L}(0)$.

In other words, W_i^+ is constructed by 'thickening' $\mathcal{F}^{m_{i-1}}(\mathscr{D}^u_{i-1})$ in the center-stable directions, and W_i^- is constructed by 'thickening' $\mathcal{F}^{-n_i}(\mathscr{D}^s_{i+1})$ in the center-unstable directions.

We define the exit and entry sets of these windows as follows:

$$\begin{aligned}
\left(W_i^+\right)^{\mathrm{ex}} =& \partial\left[B^u_{\rho_L}(0)\right] \times B^s_{\rho_S}(\boldsymbol{z}_i^+) \times B^c_{r_i}(\boldsymbol{x}_i),\\
\left(W_i^+\right)^{\mathrm{en}} =& B^u_{\rho_L}(0) \times \partial\left[B^s_{\rho_S}(\boldsymbol{z}_i^+) \times B^c_{r_i}(\boldsymbol{x}_i)\right]\\
\left(W_i^-\right)^{\mathrm{ex}} =& \partial\left[B^u_{\rho_S}(\boldsymbol{z}_i^-)\right] \times B^s_{\rho_L}(0) \times B^c_{r_i}(\boldsymbol{x}_i)\\
\left(W_i^-\right)^{\mathrm{en}} =& B^u_{\rho_S}(\boldsymbol{z}_i^-) \times \partial\left[B^s_{\rho_L}(0) \times B^c_{r_i}(\boldsymbol{x}_i)\right].
\end{aligned} \tag{693}$$

Note that the topologically stable direction of the windows comprises both the hyperbolic stable direction and the center directions.

There exist $M_{\max} > M_{\min}$ and $\rho_L > \rho_S$ with $\rho_L < \varepsilon$, such that, if $M_i = m_i + n_i$ satisfies $M_{\min} \le M_i = m_i + n_i \le M_{max}$ we have:

- $B^u_{\rho_L}(0) \times B^s_{\rho_S}(\boldsymbol{z}_i^+)$ is correctly aligned under the identity $\mathrm{Id}_{x,y}$ with $B^u_{\rho_S}(\boldsymbol{z}_i^-) \times B^s_{\rho_L}(0)$;
- $B^u_{\rho_S}(\boldsymbol{z}_i^-) \times B^s_{\rho_L}(0)$ is correctly aligned under $\mathrm{Pr}_{x,y} \circ \mathcal{F}^{m_i+n_i}(\cdot,\cdot,\boldsymbol{x}_i)$ with $B^u_{\rho_L}(0) \times B^s_{\rho_S}(\boldsymbol{z}_{i+1}^+)$.

For m_i, n_i fixed as above, by the construction of the sequence of balls at the beginning of the proof, there exist $r_1, \dots, r_N$ such that $B_{r_i}(\boldsymbol{x}_i)$ is correctly aligned with $B_{r_{i+1}}(\boldsymbol{x}_{i+1})$ under the transition map τ_i, in the sense that

$$\tau_i(B_{r_i}(\boldsymbol{x}_i)) \subset B_{r_{i+1}}(\boldsymbol{x}_{i+1}). \tag{703}$$

The correct alignment of the hyperbolic components and that of the center components of the windows do not automatically imply that correct alignment of the full windows. Therefore, we choose r_1 (and implicitly $r_2, \dots, r_N$) so that

- $B^u_{\rho_S}(\boldsymbol{z}_i^-) \times B^s_{\rho_L}(0)$ is correctly aligned under $\mathrm{Pr}_{x,y} \circ \mathcal{F}^{m_i+n_i}(\cdot,\cdot,\boldsymbol{y})$ with $B^u_{\rho_L}(0) \times B^s_{\rho_S}(\boldsymbol{z}_{i+1}^+)$ for all $\boldsymbol{x} \in B^c_{r_i}(\boldsymbol{x}_i)$.

Therefore, we obtain, for all $i = 1, \dots, N-1$,

- W_i^+ is correctly aligned under the identity Id with W_i^-;
- W_i^- is correctly aligned under $\mathcal{F}^{n_i+m_i}$ with W_{i+1}^+;

See Fig. 4.

In addition, we choose r_1 so that all $r_1, \dots, r_N$ are less than $\varepsilon > 0$.

Then, by the property of correctly aligned windows[1] there exists $\boldsymbol{y}_1$ whose orbit $\boldsymbol{y}_1, \dots, \boldsymbol{y}_N$ satisfies

$$\begin{aligned}
\boldsymbol{y}_{i+1} =& \mathcal{F}^{M_i}(\boldsymbol{y}_i), \text{ for } i = 1, \dots, N-1, \text{ and}\\
\boldsymbol{y}_i \in& W_i^+ \cap W_i^-, \text{ for } i = 1, \dots, N.
\end{aligned} \tag{716}$$

In particular, the orbit $\boldsymbol{y}_1, \dots, \boldsymbol{y}_N$ ε-shadows $\boldsymbol{x}_1, \dots, \boldsymbol{x}_N$, as desired.

7.2. Proof of Theorem 3.2. We consider the BNF system given by $\mathcal{Z}$. Let $\tilde{\Phi}_t$ denote the flow of $\mathcal{Z}$, $\mathcal{F}$ be the first return map to Σ, and $f = \mathcal{F}_{|\Lambda}$.

[1] If $\{W_i\}_{i\in\mathbb{Z}}$ is a sequence of windows in $\mathbb{R}^n$ with unstable-like dimension n_u and stable-like dimension n_s, such that $n_u + n_s = n$, and W_i is correctly aligned with W_{i+1} under $\mathcal{F}$ for all i, then there exists an orbit $\{\boldsymbol{y}_i\}_{i\in\mathbb{Z}}$ of $\mathcal{F}$ such that $\boldsymbol{y}_i \in W_i$ and $\boldsymbol{y}_{i+1} = \mathcal{F}(\boldsymbol{y}_i)$ for all i [44].

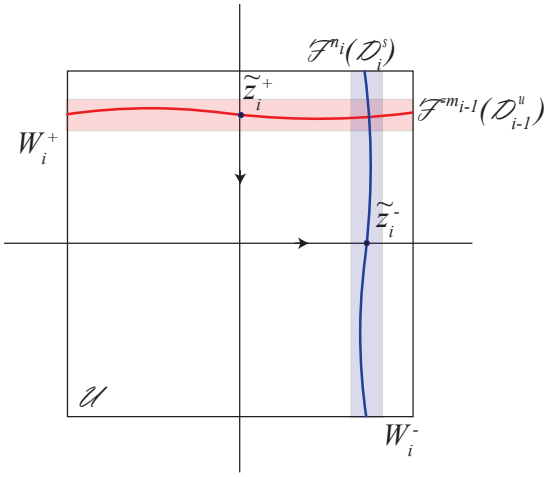


Figure 4: Correctly aligned windows near Λ.

Let $(\boldsymbol{x}_i)_{i=1}^N$ be a guiding orbit in Σ of the iterated function system (IFS) generated by the transition maps $\{\tau_1, \dots, \tau_{N-1}\}$, such that

$$\boldsymbol{x}_{i+1} = \tau_i(\boldsymbol{x}_i)$$

where

$$\tau_i = f^{m_*} \circ \sigma_{\alpha(i)} \circ f^{n_*},$$

for $i = 1, \dots, N-1$. Let $\varepsilon > 0$ be arbitrarily small. By Lemma 2.6 there exist m_*, n_* sufficiently large such that, for the guided orbit $(\boldsymbol{x}_i)_{i=1}^N$ of the corresponding transition maps, there is an orbit of the first return map $\mathcal{F}$ to Σ such that

$$d(\boldsymbol{x}_i, \mathcal{F}^{M_*}(\boldsymbol{x}_i)) < \varepsilon,$$

where $M_* = m_* + n_*$.

Consequently, there exists a trajectory $\tilde{\Phi}_t(\boldsymbol{x})$ of the system given by $\mathcal{Z}$ that ε-shadows $(\boldsymbol{x}_i)_{i=1}^N$, i.e., there exists an sequence of times $0 < t_1 < \ldots < t_N$ such that

$$d(\boldsymbol{x}_i, \tilde{\Phi}_{t_i}(\boldsymbol{x})) < \varepsilon, \text{ for } i = 1, \dots, N. \tag{7.1}$$

Since the system $\mathcal{Z}$ is ϵ_M-close to the original system H, by Gronwall's inequality, there exists a constant C_0 such that

$$d(\Phi_t(\boldsymbol{x}), \tilde{\Phi}_t(\boldsymbol{x})) < \epsilon_M e^{C_0 t}, \text{ for } t > 0. \tag{7.2}$$

Then, for $C = 1 + e^{C_0 t_N}$, from (7.1) and (7.2), we obtain

$$d(\boldsymbol{x}_i, \Phi_{t_i}(\boldsymbol{x})) < \varepsilon + \epsilon_M C, \text{ for } i = 1, \dots, N.$$

8. General error estimates for the BNF. After a translation and a symplectic linear change of variables

$$(X, Y, Z, P_X, P_Y, P_Z) = L + C(Q, P) = L + C(Q_1, Q_2, Q_3, P_1, P_2, P_3),$$

the Hamiltonian of a general saddle-center-center takes the form $H = H_2 + O_3$, where the quadratic part H_2 is already in its real normal form, which is formula (14.8) in [22]

$$H_2 = \lambda^0 Q_1 P_1 + \frac{\nu_{\mathrm{p}}^0}{2}\left(Q_2^2 + P_2^2\right) + \frac{\nu_{\mathrm{v}}^0}{2}\left(Q_3^2 + P_3^2\right).$$

We can construct the BNF of order $M \geq 2$ provided that the so called *small divisors* associated with the equilibrium point L remain strictly positive for all $s = 2, \dots, M$. These small divisors are defined as follows:

$$\alpha_s = \alpha_s(\mu) = \min \left| k_{\mathrm{s}} \lambda^0 + i \left(k_{\mathrm{p}} \nu_{\mathrm{p}}^0 + k_{\mathrm{v}} \nu_{\mathrm{v}}^0 \right) \right| = \min \sqrt{k_{\mathrm{s}}^2 \left(\lambda^0 \right)^2 + \left(k_{\mathrm{p}} \nu_{\mathrm{p}}^0 + k_{\mathrm{v}} \nu_{\mathrm{v}}^0 \right)^2} > 0, \tag{8.1}$$

where the minimum is taken over all $k_{\mathrm{s}}, k_{\mathrm{p}}, k_{\mathrm{v}} \in \mathbb{Z}$ so that $0 < |k_{\mathrm{s}}| + |k_{\mathrm{p}}| + |k_{\mathrm{v}}| \leq s$. By definition, these small divisors form a non-increasing sequence $\alpha_2 \geq \alpha_3 \geq \cdots \geq \alpha_M$.

Then, there exists a symplectic analytic change $(Q, P) = \Psi^{(M)}(q, p)$ such that

$$\mathcal{H}^{(M)} := H \circ \Psi^{(M)} = H_2 + \mathcal{Z}^{(M)}(I) + \mathcal{R}^{(M)}(q, p),$$

with

$$\mathcal{Z}^{(M)}(\boldsymbol{I}) = \sum_{\substack{s \text{ even} \\ 4 \leq s \leq M}} \mathcal{Z}_s(\boldsymbol{I}), \quad \mathcal{R}^{(M)}(q, p) = \sum_{s \geq M+1} \mathcal{R}_s^{(M)}(q, p),$$

where $\mathcal{Z}_s(\boldsymbol{I})$ is a homogeneous polynomial of degree $s/2$ in the "action" variables $\boldsymbol{I} = (I_{\mathrm{s}}, I_{\mathrm{p}}, I_{\mathrm{v}})$, where $I_{\mathrm{s}} = xy$, with $x = q_1$, $y = p_1$, $I_{\mathrm{p}} = \dfrac{q_2^2 + p_2^2}{2}$, $I_{\mathrm{v}} = \dfrac{q_3^2 + p_3^2}{2}$, and $\mathcal{R}_s^{(M)}(q, p)$ is a homogeneous polynomial of degree s in variables (q, p).

In dealing with normal forms near a fixed point of a Hamiltonian system, it is usual to consider complex variables (X, Y) for the variables (Q, P), and to introduce the complex normal form of the quadratic part of H. The complex canonical coordinates (X, Y) are defined by the linear change

$$X_1 = q_1, \quad Y_1 = p_1, \qquad X_j = \frac{1}{\sqrt{2}} \left(q_j - \mathrm{i}\, p_j \right), \quad Y_j = -\frac{1}{\sqrt{2}} \left(q_j + \mathrm{i}\, p_j \right), \qquad j = 2, 3,$$

so that the complex normal form of H_2 becomes

$$H_2 = \lambda^0 X_1 Y_1 + \mathrm{i}\, \nu_{\mathrm{p}}^0 X_2 Y_2 + \mathrm{i}\, \nu_{\mathrm{v}}^0 X_3 Y_3. \tag{8.2}$$

The following proposition is adapted from [25, Proposition 1], which exclusively addresses the totally elliptic case; nevertheless, the formal computations remain completely analogous. Alternative bounds for the normal form terms and the remainder can be found in [10, 32, 40]. Furthermore, the sizes of all variables are uniform; consequently, the results of Proposition 8.1 apply when $\delta = r$ within the neighborhood $U = U(\delta, r)$ defined in (4.2) where the BNF is established.

Proposition 8.1. *Let $a = 20$ and $b = 548 \cdot 3$. Let $H(X, Y) = \sum_{s \geqslant 2} H_s(X, Y)$ with H_2 given in (8.2) and $\|H_s\| \leq c^{s-2} d$ for $s \geq 2$. Assume that the lower bounds for the resonances α_s given in (8.1) satisfy $\alpha_s > 0$ for $2 \leq s \leq M$. Then*

a) $\|\mathcal{Z}_s\| \leq \dfrac{\frac{1}{6}(6cd)^{s-2}(s-2)!}{\alpha_3 \cdots \alpha_{s-1}}$ *for s even, $4 \leq s \leq M$,*

b) $\left\| \mathcal{R}_s^{(M)} \right\| \leq \dfrac{ad^2 (acd)^{s-2} (M-3)! (M-2)^{s-M+2}}{\alpha_3 \cdots \alpha_{M-1} \alpha_M^{s-M+2}}$ *for $s \geq M+1$,*

c) Defining $r_M^* = \dfrac{\alpha_M}{bcdM}$, $\Psi^{(M)}$ is analytic on $\hat{\mathcal{B}}_{r_R^*}$ and, for any $r \leq r_R^*$, one has the inclusion $\Psi^{(M)}(\mathcal{B}_r) \supset \mathcal{B}_{r/2}$.

It remains to specify the norms and neighborhoods used, which are:

$$\|H_s\| := \sum_{|\beta+\beta'|_1=s} \left|H_{\beta,\beta'}\right| \text{ for } H_s(X,Y) = \sum_{|\beta+\beta'|_1=s} H_{\beta,\beta'} X^\beta Y^{\beta'},$$

$$\mathcal{B}_r := \left\{(q,p) \in \mathbb{R}^6 : |(q,p)| \le r\right\}, \text{ with } |(q,p)| := \max_{\ell=1,2,3} \sqrt{q_\ell^2 + p_\ell^2},$$

$$\hat{\mathcal{B}}_r :== \left\{(X,Y) \in \mathbb{C}^6 : |(X,Y)| \le r, (X_1,Y_1) \in \mathbb{R}^2, \bar{Y}_j = \mathrm{i}\, X_j, j = 2,3\right\},$$

$$\text{with } |(X,Y)| = \max_{\ell=1,2,3} \sqrt{|X_\ell|^2 + |Y_\ell|^2},$$

$$|f|_r := \max_{(X,Y)\in\hat{\mathcal{B}}_r} |f(X,Y)| \text{ for a function } f(X,Y).$$

Notice that given $f = \sum_s f_s$, then $|f|_r \le \sum_s \|f_s\| r^s$, and that if there exists A, B such that $\|f_s\| \le A^s B$ for all s, then f is analytic on $\hat{\mathcal{B}}_r$ for $r < 1/A$. Therefore

$$\left|\mathcal{R}^{(M)}\right|_r \le \sum_{s\ge M+1} \left\|\mathcal{R}_s^{(M)}\right\| r^s = \frac{(M-3)!}{ac^2(M-2)^{M-2}} \frac{\alpha_M^{M-2}}{\alpha_3\cdots\alpha_{M-1}} \sum_{s\ge M+1} \left(\frac{acd(M-2)}{\alpha_M} r\right)^s,$$

which is a convergent series for $r < \dfrac{\alpha_M}{acd(M-2)}$, in which case we have

$$\left|\mathcal{R}^{(M)}\right|_r \le \epsilon_M := \frac{(M-3)!}{ac^2(M-2)^{M-2}} \cdot \frac{\alpha_M^{M-2}}{\alpha_3\cdots\alpha_{M-1}} \cdot \frac{\left(\dfrac{acd(M-2)}{\alpha_M} r\right)^{M+1}}{1 - \dfrac{acd(M-2)}{\alpha_M} r}. \tag{8.3}$$

Remark 1 One can use Stirling's formula $n! = \sqrt{2\pi n}\left(\frac{n}{e}\right)^n \left(1 + O\left(\frac{1}{n}\right)\right)$ to get

$$\frac{(M-3)!}{(M-2)^{M-2}} = \frac{(M-3)}{\mathrm{e}^{M-2}} \left(1 + O\left(\frac{1}{M-2}\right)\right).$$

Remark 2 $\dfrac{\alpha_M^{M-2}}{\alpha_3\cdots\alpha_{M-1}} = \dfrac{\alpha_M}{\alpha_3} \cdots \dfrac{\alpha_M}{\alpha_{M-1}} \le 1.$

In the companion paper [3], we evaluate the analytical bounds given in Proposition 8.1 for the case of the Lagrange equilibrium point L_1 in the Sun-Earth Spatial Restricted Three-Body Problem. For this particular case, we also compute numerically the BNF up to degree M=16. In this way, we can explicitly compute the norms $\|\mathcal{Z}_s\|, \|\mathcal{R}_s\|$ and compare them with their theoretical bounds.

REFERENCES

[1] S. W. Akingbade, M. Gidea, and T. M-Seara, *Arnold diffusion in a model of dissipative system*, SIAM J. Appl. Dyn. Syst., 22 (2023), pp. 1983–2023, https://doi.org/10.1137/22M1525508, https://doi.org/10.1137/22M1525508.

[2] E. M. Alessi, I. Baldomá, M. Giralt, and M. Guardia, *On the Arnold diffusion mechanism in medium Earth orbit*, J. Nonlinear Sci., 35 (2025), pp. Paper No. 8, 54, https://doi.org/10.1007/s00332-024-10080-0, https://doi.org/10.1007/s00332-024-10080-0.

[3] R. L. Anderson, A. Delshams, M. Gidea, and P. Roldan, *Effective shadowing of transition maps for a Hamiltonian saddle-center-center equilibrium. Part II: numerical results*. Preprint at https://web.mat.upc.edu/amadeu.delshams/articles/ADRG26SOTM2.pdf, 2026.

[4] V. Arnold, *Instability of dynamical systems with several degrees of freedom*, Sov. Math. Doklady, 5 (1964), pp. 581–585. See also *Vladimir I. Arnold—collected works. Vol. I*, Springer-Verlag, Berlin, 2009, pp. 423–427, DOI 10.1007/978-3-642-01742-1, or *Hamiltonian Dynamical Systems*, edited by R.S MacKay, J.D Meiss, CRC Press, 2020, pp. 633–637, DOI 10.1201/9781003069515.

[5] M. Berti, L. Biasco, and P. Bolle, *Drift in phase space: a new variational mechanism with optimal diffusion time*, J. Math. Pures Appl. (9), 82 (2003), pp. 613–664, https://doi.org/10.1016/S0021-7824(03)00032-1, https://doi-org.recursos.biblioteca.upc.edu/10.1016/S0021-7824(03)00032-1.

[6] A. Bounemoura, *Generic super-exponential stability of invariant tori in Hamiltonian systems*, Ergodic Theory Dynam. Systems, 31 (2011), pp. 1287–1303, https://doi.org/10.1017/S0143385710000441, https://doi-org.recursos.biblioteca.upc.edu/10.1017/S0143385710000441.

[7] J. Burgos-García, M. Gidea, and C. Sierpe, *Arnold diffusion in the elliptic Hill four-body problem: geometric method and numerical verification*, Nonlinearity, 38 (2025), pp. Paper No. 095016, 51, https://doi.org/10.1088/1361-6544/adfff8, https://doi.org/10.1088/1361-6544/adfff8.

[8] X. Cabré, E. Fontich, and R. de la Llave, *The parameterization method for invariant manifolds. III. Overview and applications*, J. Differential Equations, 218 (2005), pp. 444–515, https://doi.org/10.1016/j.jde.2004.12.003, https://doi-org.recursos.biblioteca.upc.edu/10.1016/j.jde.2004.12.003.

[9] M. J. Capiński and M. Gidea, *Arnold diffusion, quantitative estimates, and stochastic behavior in the three-body problem*, Comm. Pure Appl. Math., 76 (2023), pp. 616–681, https://doi.org/10.1002/cpa.22014, https://doi.org/10.1002/cpa.22014.

[10] C. Caracciolo and U. Locatelli, *Computer-assisted estimates for Birkhoff normal forms*, J. Comput. Dyn., 7 (2020), pp. 425–460, https://doi.org/10.3934/jcd.2020017, https://doi-org.recursos.biblioteca.upc.edu/10.3934/jcd.2020017.

[11] Q. Chen and R. de la Llave, *Analytic genericity of diffusing orbits in a priori unstable Hamiltonian systems*, Nonlinearity, 35 (2022), pp. 1986–2019, https://doi.org/10.1088/1361-6544/ac50bb, https://doi.org/10.1088/1361-6544/ac50bb.

[12] A. Clarke, *Geodesics with unbounded speed on fluctuating surfaces*, Regul. Chaotic Dyn., 29 (2024), pp. 435–450, https://doi.org/10.1134/S1560354724030018, https://doi.org/10.1134/S1560354724030018.

[13] A. Clarke, J. Fejoz, and M. Guardia, *A counterexample to the theorem of Laplace-Lagrange on the stability of semimajor axes*, Arch. Ration. Mech. Anal., 248 (2024), pp. Paper No. 19, 73, https://doi.org/10.1007/s00205-024-01960-6, https://doi.org/10.1007/s00205-024-01960-6.

[14] A. Clarke, J. Fejoz, and M. Guardia, *Why are inner planets not inclined?*, Publ. Math. Inst. Hautes Études Sci., 141 (2025), pp. 1–98, https://doi.org/10.1007/s10240-024-00151-z, https://doi.org/10.1007/s10240-024-00151-z.

[15] A. Clarke and D. Turaev, *Arnold diffusion in multidimensional convex billiards*, Duke Math. J., 172 (2023), pp. 1813–1878, https://doi.org/10.1215/00127094-2022-0073, https://doi.org/10.1215/00127094-2022-0073.

[16] A. Delshams, R. de la Llave, and T. M. Seara, *A geometric approach to the existence of orbits with unbounded energy in generic periodic perturbations by a potential of generic geodesic flows of* $\mathbf{T}^2$, Comm. Math. Phys., 209 (2000), pp. 353–392, https://doi.org/10.1007/PL00020961, https://doi.org/10.1007/PL00020961.

[17] A. Delshams, R. de la Llave, and T. M. Seara, *A geometric mechanism for diffusion in Hamiltonian systems overcoming the large gap problem: heuristics and rigorous verification on a model*, Mem. Amer. Math. Soc., 179 (2006), pp. viii+141, https://doi.org/10.1090/memo/0844, https://doi.org/10.1090/memo/0844.

[18] A. Delshams, R. de la Llave, and T. M. Seara, *Orbits of unbounded energy in quasi-periodic perturbations of geodesic flows*, Adv. Math., 202 (2006), pp. 64–188, https://doi.org/10.1016/j.aim.2005.03.005, https://doi.org/10.1016/j.aim.2005.03.005.

[19] A. Delshams, R. de la Llave, and T. M. Seara, *Geometric properties of the scattering map of a normally hyperbolic invariant manifold*, Adv. Math., 217 (2008), pp. 1096–1153, https://doi.org/10.1016/j.aim.2007.08.014, https://doi.org/10.1016/j.aim.2007.08.014.

[20] A. Delshams, R. de la Llave, and T. M. Seara, *Instability of high dimensional Hamiltonian systems: multiple resonances do not impede diffusion*, Adv. Math., 294 (2016), pp. 689–755, https://doi.org/10.1016/j.aim.2015.11.010, https://doi.org/10.1016/j.aim.2015.11.010.

[21] A. Delshams, M. Gidea, and P. Roldán, *Transition map and shadowing lemma for normally hyperbolic invariant manifolds*, Discrete Contin. Dyn. Syst., 33 (2013), pp. 1089–1112, https://doi.org/10.3934/dcds.2013.33.1089, https://doi-org.recursos.biblioteca.upc.edu/10.3934/dcds.2013.33.1089.

[22] A. Delshams, M. Gidea, and P. Roldan, *Arnold's mechanism of diffusion in the spatial circular restricted three-body problem: a semi-analytical argument*, Phys. D, 334 (2016), pp. 29–48, https://doi.org/10.1016/j.physd.2016.06.005, https://doi-org.recursos.biblioteca.upc.edu/10.1016/j.physd.2016.06.005.

[23] A. Delshams, M. Gidea, and P. Roldan, *Semi-analytic construction of global transfers between quasi-periodic orbits in the spatial R3BP*, Commun. Nonlinear Sci. Numer. Simul., 152 (2026), pp. Paper No. 109220, 34, https://doi.org/10.1016/j.cnsns.2025.109220, https://doi-org.recursos.biblioteca.upc.edu/10.1016/j.cnsns.2025.109220.

[24] A. Delshams, A. Granados, and R. G. Schaefer, *Arnold diffusion for an a priori unstable Hamiltonian system with* $3 + 1/2$ *degrees of freedom*, Chaos, 34 (2024), pp. Paper No. 063118, 17, https://doi.org/10.1063/5.0185044, https://doi.org/10.1063/5.0185044.

[25] A. Delshams and P. Gutiérrez, *Estimates on invariant tori near an elliptic equilibrium point of a Hamiltonian system*, J. Differential Equations, 131 (1996), pp. 277–303, https://doi.org/10.1006/jdeq.1996.0165, https://doi-org.recursos.biblioteca.upc.edu/10.1006/jdeq.1996.0165.

[26] A. Delshams and G. Huguet, *Geography of resonances and Arnold diffusion in a priori unstable Hamiltonian systems*, Nonlinearity, 22 (2009), pp. 1997–2077, https://doi.org/10.1088/0951-7715/22/8/013, https://doi.org/10.1088/0951-7715/22/8/013.

[27] A. Delshams and G. Huguet, *A geometric mechanism of diffusion: rigorous verification in a priori unstable Hamiltonian systems*, J. Differential Equations, 250 (2011), pp. 2601–2623, https://doi.org/10.1016/j.jde.2010.12.023, https://doi.org/10.1016/j.jde.2010.12.023.

[28] A. Delshams, V. Kaloshin, A. de la Rosa, and T. M. Seara, *Global instability in the restricted planar elliptic three body problem*, Comm. Math. Phys., 366 (2019), pp. 1173–1228, https://doi.org/10.1007/s00220-018-3248-z, https://doi.org/10.1007/s00220-018-3248-z.

[29] A. Delshams and R. G. Schaefer, *Arnold diffusion for a complete family of perturbations*, Regul. Chaotic Dyn., 22 (2017), pp. 78–108, https://doi.org/10.1134/S1560354717010051, https://doi.org/10.1134/S1560354717010051.

[30] A. Delshams and R. G. Schaefer, *Arnold diffusion for a complete family of perturbations with two independent harmonics*, Discrete Contin. Dyn. Syst., 38 (2018), pp. 6047–6072, https://doi.org/10.3934/dcds.2018261, https://doi.org/10.3934/dcds.2018261.

[31] A. Delshams and K. Zhang, *Generic global diffusion for analytic a priori unstable systems*, Comm. Math. Phys., 406 (2025), pp. Paper No. 146, 22, https://doi.org/10.1007/s00220-025-05342-1, https://doi.org/10.1007/s00220-025-05342-1.

[32] C. Efthymiopoulos, A. Giorgilli, and G. Contopoulos, *Nonconvergence of formal integrals. II. Improved estimates for the optimal order of truncation*, J. Phys. A, 37 (2004), pp. 10831–10858, https://doi.org/10.1088/0305-4470/37/45/008, https://doi-org.recursos.biblioteca.upc.edu/10.1088/0305-4470/37/45/008.

[33] E. Fontich and P. Martín, *Arnold diffusion in perturbations of analytic integrable Hamiltonian systems*, Discrete Contin. Dynam. Systems, 7 (2001), pp. 61–84, https://doi.org/10.3934/dcds.2001.7.61, https://doi-org.recursos.biblioteca.upc.edu/10.3934/dcds.2001.7.61.

[34] V. Gelfreich and D. Turaev, *Arnold diffusion in a priori chaotic symplectic maps*, Communications in Mathematical Physics, 353 (2017), pp. 507–547, https://doi.org/10.1007/s00220-017-2867-0, https://doi.org/10.1007/s00220-017-2867-0.

[35] M. Gidea and R. de la Llave, *Global Melnikov theory in Hamiltonian systems with general time-dependent perturbations*, J. Nonlinear Sci., 28 (2018), pp. 1657–1707, https://doi.org/10.1007/s00332-018-9461-2, https://doi.org/10.1007/s00332-018-9461-2.

[36] M. Gidea, R. de la Llave, and T. M-Seara, *A general mechanism of diffusion in Hamiltonian systems: qualitative results*, Comm. Pure Appl. Math., 73 (2020), pp. 150–209, https://doi.org/10.1002/cpa.21856, https://doi.org/10.1002/cpa.21856.

[37] M. Gidea, R. de la Llave, and T. M. Seara, *A general mechanism of instability in Hamiltonian systems: skipping along a normally hyperbolic invariant manifold*, Discrete Contin. Dyn. Syst., 40 (2020), pp. 6795–6813, https://doi.org/10.3934/dcds.2020166, https://doi.org/10.3934/dcds.2020166.

[38] A. Giorgilli, A. Delshams, E. Fontich, L. Galgani, and C. Simó, *Effective stability for a Hamiltonian system near an elliptic equilibrium point, with an application to the restricted three-body problem*, J. Differential Equations, 77 (1989), pp. 167–198, https://doi.org/10.1016/0022-0396(89)90161-7, https://doi-org.recursos.biblioteca.upc.edu/10.1016/0022-0396(89)90161-7.

[39] M. Guardia, J. Paradela, and T. M. Seara, *A degenerate Arnold diffusion mechanism in the restricted 3-body problem*, Ann. Sci. Éc. Norm. Supér. (4), 58 (2025), pp. 1401–1478, https://doi.org/10.24033/asens.2632, https://doi.org/10.24033/asens.2632.

[40] M. Guzzo, C. Caracciolo, and G. Pinzari, *Improved stability estimates at elliptic equilibria of hamiltonian systems*, Discrete Contin. Dyn. Syst., 77 (2026), pp. 1–31, https://doi.org/10.3934/dcds.2026063, https://www.aimsciences.org/article/id/69bbb40cd1a02b472f36a46e.

[41] A. Haro, M. Canadell, J.-L. Figueras, A. Luque, and J.-M. Mondelo, *The parameterization method for invariant manifolds*, vol. 195 of Applied Mathematical Sciences, Springer, [Cham], 2016, https://doi.org/10.1007/978-3-319-29662-3, https://doi-org.recursos.biblioteca.upc.edu/10.1007/978-3-319-29662-3. From rigorous results to effective computations.

[42] A. Jorba and J. Masdemont, *Dynamics in the center manifold of the collinear points of the restricted three body problem*, Phys. D, 132 (1999), pp. 189–213, https://doi.org/10.1016/S0167-2789(99)00042-1, https://doi.org/10.1016/S0167-2789(99)00042-1.

[43] D. Treschev, *Evolution of slow variables in a priori unstable Hamiltonian systems*, Nonlinearity, 17 (2004), pp. 1803–1841.

[44] P. Zgliczyński and M. Gidea, *Covering relations for multidimensional dynamical systems*, Journal of Differential Equations, 202 (2004), pp. 32–58.